Nanoscale

REVIEW

View Article Online
View Journal | View Issue

Cite this: *Nanoscale*, 2026, **18**, 10503

Mechanisms and potential applications of technologies for detecting specific polyfluoroalkyl substances *via* nano-level interactions

Aki Shibata, *[a] Mitsuaki Nuno,[b] Tomoka Ishikawa,[a] Hitoshi Kasai [a] and Kouki Oka *[a,c,d]

Per- and polyfluoroalkyl substances, possessing chemically and thermally stable C–F bonds, have been widely used in various products owing to their flame retardancy, chemical resistance, and water- and oil-repellent characteristics. Among these, some perfluoroalkyl substances ('specific PFASs') are beginning to raise concerns regarding their potential toxicity to living organisms and bioaccumulation. Recently, specific PFASs originating from fire-extinguishing foam, wastewater from semiconductor manufacturing plants, and fluororesin-coated waste have been detected in aqueous environments worldwide. These species are mainly present at low concentrations (parts-per-trillion (ppt) level) and have prompted stringent regulations, such as drinking water standards. Liquid chromatography–tandem mass spectrometry remains the gold standard for detecting specific PFASs at the ppt level. However, its implementation necessitates skilled handling and long analysis durations. To address these problems, based on interactions with specific PFASs at the nano-level, there has been active development of materials aimed at detecting specific PFASs with high sensitivity, in a simple manner, and in a short time. Several materials capable of detecting specific PFASs at parts-per-billion (ppb) to parts-per-million (ppm) levels are already undergoing verification research with a view to practical application. Nevertheless, the detection of specific PFASs at the ppt level in actual aqueous environments remains challenging owing to limited selectivity against contaminants and difficulty in widespread on-site detection. This review provides a comprehensive overview of detection materials and technologies for specific PFASs. Moreover, it comprehensively discusses the detection mechanisms and sensing performance of specific PFAS detection materials, as well as issues facing practical application, and presents future prospects for materials and their development aimed at the simple, rapid, and highly sensitive detection of specific PFASs.

Received 31st December 2025,
Accepted 29th March 2026

DOI: 10.1039/d5nr05521k

rsc.li/nanoscale

1. Introduction

PFASs is a general term for fluorinated substances that contain at least one fully fluorinated methyl or methylene carbon atom.[1–3] Among these compounds, those with a hydrophobic methylene backbone and hydrophilic terminal functional groups (*e.g.*, –COOH and –SO_3H) exhibit surfactant properties (Fig. 1).[4–6] PFASs have been extensively used in a wide range of industrial and consumer products, including fire-extinguishing foams, semiconductor manufacturing, water-repellent coatings, and food packaging, due to their flame retardancy, chemical resistance, and water and oil repellency, which stem from their inertness, high durability, and the low surface energy of the C–F bond.[7–17] In contrast, certain PFASs ('specific

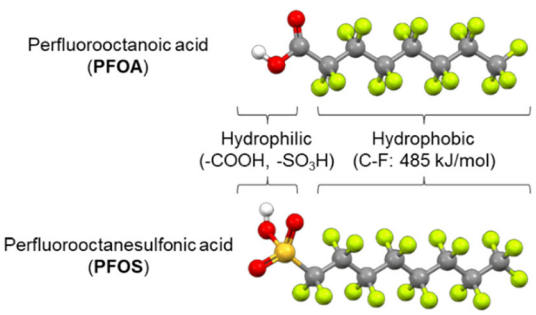

Fig. 1 Chemical structures of representative 'specific PFASs', such as PFOA and PFOS (hydrophilic moieties: –COOH and –SO_3H; hydrophobic moiety: a carbon chain with a C–F bond (485 kJ mol^{-1})).

[a]*Institute of Multidisciplinary Research for Advanced Materials, Tohoku University, 2-1-1 Katahira, Aoba-ku, Sendai, Miyagi 980-8577, Japan. E-mail: oka@tohoku.ac.jp, aki.shibata.d5@tohoku.ac.jp*
[b]*Kubota Corporation, 1-1-1, Hama, Amagasaki, Hyogo 661-8567, Japan*
[c]*Carbon Recycling Energy Research Center, Ibaraki University, 4-12-1, Nakanarusawacho, Hitachi, Ibaraki 316-0033, Japan*
[d]*Deuterium Science Research Unit, Center for the Promotion of Interdisciplinary Education and Research, Kyoto University, Yoshida, Sakyo-ku, Kyoto 606-8501, Japan*

PFASs') emitted, leaked or leached from manufacturing facilities and waste products have been increasingly detected in public water bodies and groundwater through wastewater discharge and precipitation.[18–22] The C–F bond in PFASs exhibits the highest bond dissociation energy (approximately 485 kJ mol^{-1}) among covalent single bonds in organic compounds, which renders it extremely chemically and thermally stable.[23–26] Consequently, PFASs are highly resistant to decomposition in aqueous environments and persist as 'forever chemicals'.[27,28]

In recent years, living organisms have been exposed to PFAS through drinking and domestic water.[29–33] Specific PFASs,[34,35] such as perfluorooctanoic acid (PFOA) and perfluorooctanesulfonic acid (PFOS), have raised concerns about their potential for toxicity to living organisms, including carcinogenicity,[36,37] immunosuppression,[38,39] endocrine disruption,[40,41] and bioaccumulation.[42–47] In particular, these specific PFASs have been reported to be present at high concentrations (several ppm levels) in water bodies near certain areas such as fire training grounds and semiconductor manufacturing plants.[48,49] Consequently, many countries worldwide have begun regulating the concentrations of specific PFASs in aqueous environments, while strengthening their monitoring to promote environmental and health management. The World Health Organization has proposed a guideline limit of 100 ppt for the total concentration of PFASs in drinking water and is aiming for a strict management system.[50] Several countries have established more stringent drinking-water standards. For example, the U.S. Environmental Protection Agency (EPA) sets a limit of 4 ppt for PFOA and PFOS, respectively,[51] while Denmark has established a limit of 2 ppt for the combined concentration of PFOA, PFOS, perfluorohexanesulfonic acid, and perfluorononanoic acid (PFNA).[52]

Specific PFASs in aqueous environments are typically present at ppt levels,[53–57] necessitating ultrasensitive detection technologies. Liquid chromatography-tandem mass spectrometry (LC-MS/MS), the current gold standard, can detect specific PFASs at the ppt level.[58] However, the analysis is cost- and time-intensive (USD 200–300 per sample; half a day to more than a day to measure PFAS-containing samples (it is estimated that the process from sample collection to receiving the measurement results from the external contractor takes 2–6 weeks.)[59]) and requires expensive equipment (USD 1 000 000–2 000 000) and skilled technicians.[60,61] As regular monitoring systems for specific PFASs begin to be established globally, LC-MS/MS measurements of all water bodies and industrial sites suspected of contamination are not feasible.[62]

Based on the above, alternative detection technologies are being investigated to enable prompt, facile, and low-cost detection of specific PFAS in aqueous environments. Many of these technologies are based on nano-level interactions between the detection materials and specific PFASs (Fig. 2). This review provides a comprehensive overview of specific PFAS detection research reported in recent years, focusing on nano-level interaction-based detection mechanisms and sensing performance. This review systematically summarizes the detection mechanism of each detection research, along with its limit of detection (LOD), detection time, measurement solvent, interfering species, and detection selectivity. In addition, based on a systematic comparison of specific PFAS detection research, it discusses challenges in applying the research to actual aqueous environments and presents requirements for future development prospects.

2. Nano-level interaction-based detection of specific PFAS

Recent major research enabling rapid, low-cost, and simple detection of specific PFASs was classified based on differences in detection mechanisms. Colorimetric detection (Section 2.1) involves observing changes in absorbance due to the interaction of specific PFASs with the surface of a detection material. Fluorescence detection (Section 2.2) involves detecting changes in the excitation state of the material or the energy transfer process associated with the interaction

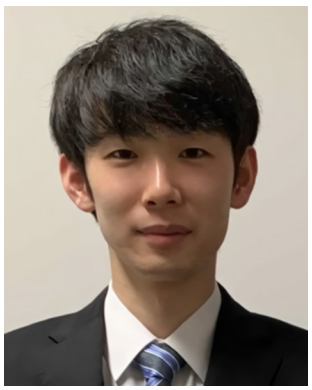

Aki Shibata

Aki Shibata is an Assistant Professor at the Institute of Multidisciplinary Research for Advanced Materials (IMRAM), Tohoku University. He received his Ph.D. degree from Tohoku University in 2025, supported by the Tohoku University Division for Interdisciplinary Advanced Research and Education (DIARE) and the Japan Society for the Promotion of Science (JSPS) Research Fellow. His research focuses on functional organic nanomaterials and nano-bioscience.

Mitsuaki Nuno

Mitsuaki Nuno is currently working as a Senior Expert in the Water and Environment R&D Dept. II at Kubota Corporation in Hyogo Prefecture. He is a researcher with expertise in water infrastructure such as water supply and sewerage facilities and water purification plants, as well as the safety management of drinking water. His research focuses on the development of water quality monitoring and water treatment technologies.

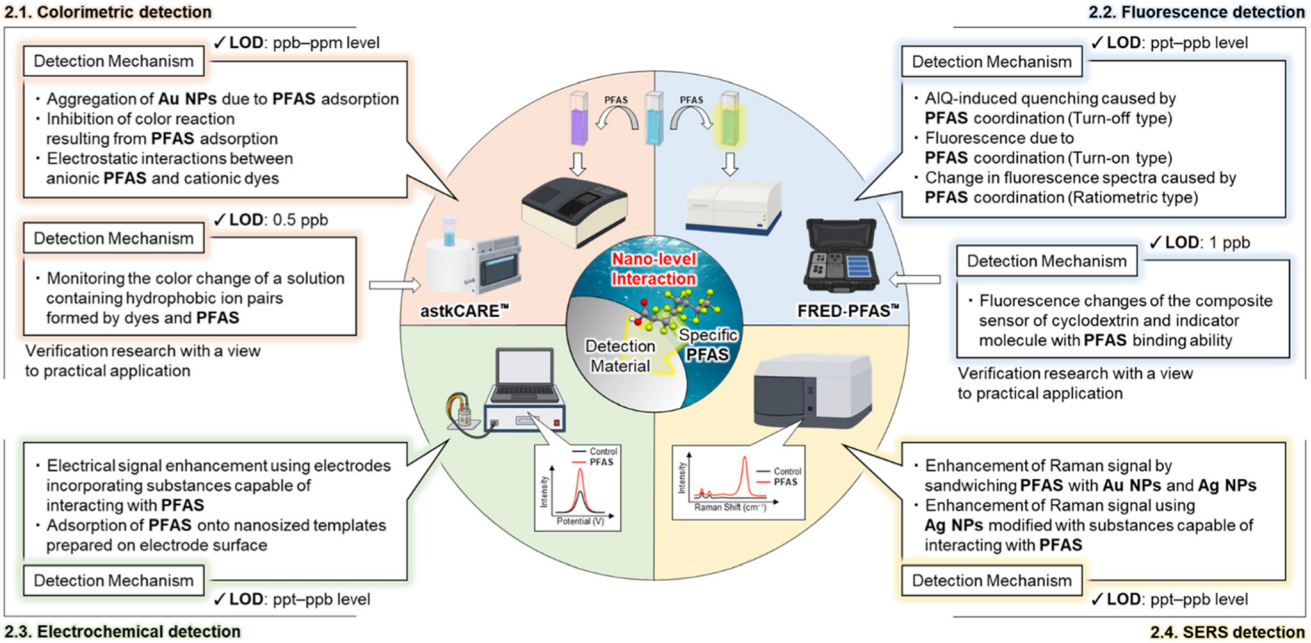

Fig. 2 Overview of specific PFAS detection technologies discussed in sections 2.1–2.4 (colorimetric, fluorescence, electrochemical, and SERS detection) and their detection mechanisms based on nanolevel interactions with specific PFASs. (Abbreviations: SERS: surface-enhanced Raman scattering; LOD: limit of detection; Au NPs: gold nanoparticles; Ag NPs: silver nanoparticles; and AIQ: aggregation-induced quenching.).

between the specific PFAS and the detection material, resulting in a fluorescence signal. Electrochemical detection (Section 2.3) involves converting the interaction between specific PFASs and nanostructures on the electrode surface into an electrical signal. Surface-enhanced Raman scattering (SERS) detection (Section 2.4) utilizes the interaction between specific PFASs and nanometal surfaces to detect vibrational spectra with high sensitivity. This review focuses on major research that utilizes the detection mechanism based on nano-level interactions with specific PFASs, and outlines the detection process for specific PFASs, the detection ability for PFAS (PFAS as a single substance such as PFOA and PFOS), the reactivity of detection materials to contaminants such as ions and surfactants, and challenges for practical application.

2.1. Colorimetric detection

Colorimetric detection based on nano-level interactions with specific PFASs can be divided into three categories, based on the [1] aggregation state of the detection material, [2] catalytic reaction of the detection material (nanozyme), and [3] absor-

Tomoka Ishikawa

Tomoka Ishikawa is a Ph.D. candidate at the Graduate School of Engineering, Tohoku University, currently conducting research under Professor Hitoshi Kasai and Associate Professor Kouki Oka. She received her Bachelor's degree from Tohoku University in 2025. Her research focuses on organic materials science and biotechnology.

Hitoshi Kasai

Hitoshi Kasai has been a Professor at the Institute of Multidisciplinary Research for Advanced Materials (IMRAM), Tohoku University, since 2016. He obtained his Ph.D. from Tohoku University in 1996 and joined the university as an Assistant Professor, becoming an Associate Professor in 2004. From 2007 to 2010, he served as a PRESTO researcher of JST. His research focuses on organic and drug-based nanocrystals and nanoparticles, pioneering carrier-free drug delivery systems with enhanced efficacy and reduced side effects. He has authored over 300 publications, including original articles, reviews, book chapters, and patents.

bance of dyes that form hydrophobic ion pairs and F–F interactions. These methods are being explored as promising strategies for the rapid and simple on-site detection of specific PFASs.

[1] In aggregation-based detection, the detection material aggregates through interaction with specific PFASs, allowing detection through changes in the absorption spectrum or visible colour (Fig. 3A).[63] This method commonly involves gold nanoparticles (Au NPs), which exhibit colour transitions between dispersed and aggregated states owing to plasmon resonance. The surface of Au NPs is typically modified with functional groups that can enhance reactivity with specific PFASs. For example, Ma *et al.* prepared cyclodextrin (CD)-modified Au NPs (CD@Au NPs) and achieved a LOD of 70.4 ppb for PFOA within 1 h (without solid-phase extraction (SPE)), leveraging host–guest interactions in a water/*N*,*N*-dimethylformamide (DMF) mixed solution.[63] Jung *et al.* synthesized citrate-coated Au NPs, which were surface-modified with perfluoroalkyl chains (carbon chain length of 6 or more).[64] In citrate-coated Au NPs, after mixing the NPs with multiple types of PFASs (perfluorohexanoic acid (PFHxA), PFNA, perfluorodecanoic acid (PFDA), and perfluorooctyl phosphonic acid (PFOPA) each as a single substance) in water, changes in the absorption spectrum over time were observed due to NP aggregation arising from different amounts of PFASs attached *via* F–F interactions with the perfluoroalkyl chains, exhibiting a LOD of 42.7–2005 ppb (without SPE). These NPs showed high reactivity to long-chain PFASs (such as PFDA and PFNA) that easily undergo F–F interactions with perfluoroalkyl chains, and the absorption spectrum immediately changed with the addition of a small amount of PFASs. Unfortunately, the selectivity of these NPs for detecting specific PFASs was low, and the increase in hydrophobic interactions due to the adsorption of dissolved organic matter other than specific PFASs and the decrease in electrostatic interactions due to changes in pH may also cause NPs to aggregate, potentially affecting the time-dependent changes in the absorption spectrum after addition of PFASs. As these detection mechanisms rely on aggregation of NPs, controlling dispersion stability – such as through surface modification of NPs using surfactants structurally dissimilar to PFASs, ensuring that aggregation occurs only upon interaction with PFASs – may potentially suppress reactivity to contaminants. Nonetheless, due to the evaluation of changes in absorbance and absorption spectrum at the same wavelength, it is expected to be difficult to distinguish between different types and concentrations of PFASs in the presence of multiple PFASs using this method. Consequently, aggregation-based methods using Au NPs typically achieve a LOD only in the tens-of-ppb range.[63,64]

[2] Catalytic-reaction-based detection uses nanozymes, composed of metal oxides or carbon materials, that catalyse the production of reactive oxygen species (ROS) (Fig. 3B).[65] Detection is accomplished by comparing the colorimetric response of 3,3′,5,5′-tetramethylbenzidine (TMB) in the presence and absence of specific PFASs. The nanozyme detects specific PFASs through the following process: (1) The colourless TMB is oxidized by ROS generated on the nanozyme surface and turns blue. (2) When specific PFASs adsorb onto the nanozyme surface, ROS generation is inhibited, and no colouration of the added TMB occurs. By comparing the colorimetric responses of TMB in steps (1) and (2), the concentration of specific PFASs can be quantified. This detection method has been actively investigated in recent years, and various nanozymes have been fabricated, including metal–organic frameworks (MOFs),[66–70] zeolitic imidazolate frameworks (ZIFs),[71] metal oxide clusters,[72] gold nanoclusters,[73] and supramolecular polymers.[74] These nanozymes can detect PFOA or PFOS (each as a single substance) in water (and in methanol, in some cases) within 1 h (without SPE), with a LOD within the range of approximately 50–400 ppb. These materials were hardly affected by contaminants such as ions (*e.g.*, Na^+, K^+, and Cl^-) found in tap water and river water, and surfactants with structures similar to specific PFAS (*e.g.*, sodium dodecyl sulfate (SDS) and sodium dodecyl benzenesulfonate (SDBS)). Because this method evaluates changes in absorbance at the same wavelength, it is expected to be difficult to distinguish between different types and concentrations of PFASs in the presence of multiple PFASs. Notably, nanozymes with improved reactivity toward specific PFASs and ROS generation capacity (*e.g.*, perfluoroalkyl-functionalized MOFs (Fe_3O_4@MON-F@Ru and PCN-222(Fe)-3F),[66,70] copper(I)–carbonitride (Cu–CN),[75] and copper-substituted cobalt-based Prussian blue derivative nanoboxes (CuCO-PBA NBs)[65]) have achieved improved LODs of approximately 6–7 ppb. Although the nanozymes structurally optimized to interact with specific PFASs by the introduction of perfluoroalkyl chains prone to F–F interactions and cavity structures that increase the specific surface area[65,66,70,75] have made substantial progress toward achieving unprecedented ppt-level LODs in the colorimetric detection of specific PFASs, their application is limited by a complicated reaction process involving multiple reagents (an

Kouki Oka

Kouki Oka has been an Associate Professor at the Institute of Multidisciplinary Research for Advanced Materials (IMRAM), Tohoku University, since April 2025. He received his Ph.D. degree from Waseda University and also received joint supervision at Uppsala University during his doctoral course. Following his Ph.D., he held a postdoctoral fellowship (PD and CPD) from the Japan Society for the Promotion of Science (JSPS) and a tenure-track position as Assistant Professor. He joined Tohoku University as a Senior Lecturer in 2023. His major interests are advanced organic functional polymers and materials for batteries, sensors, hydrogen storage, and catalysis.

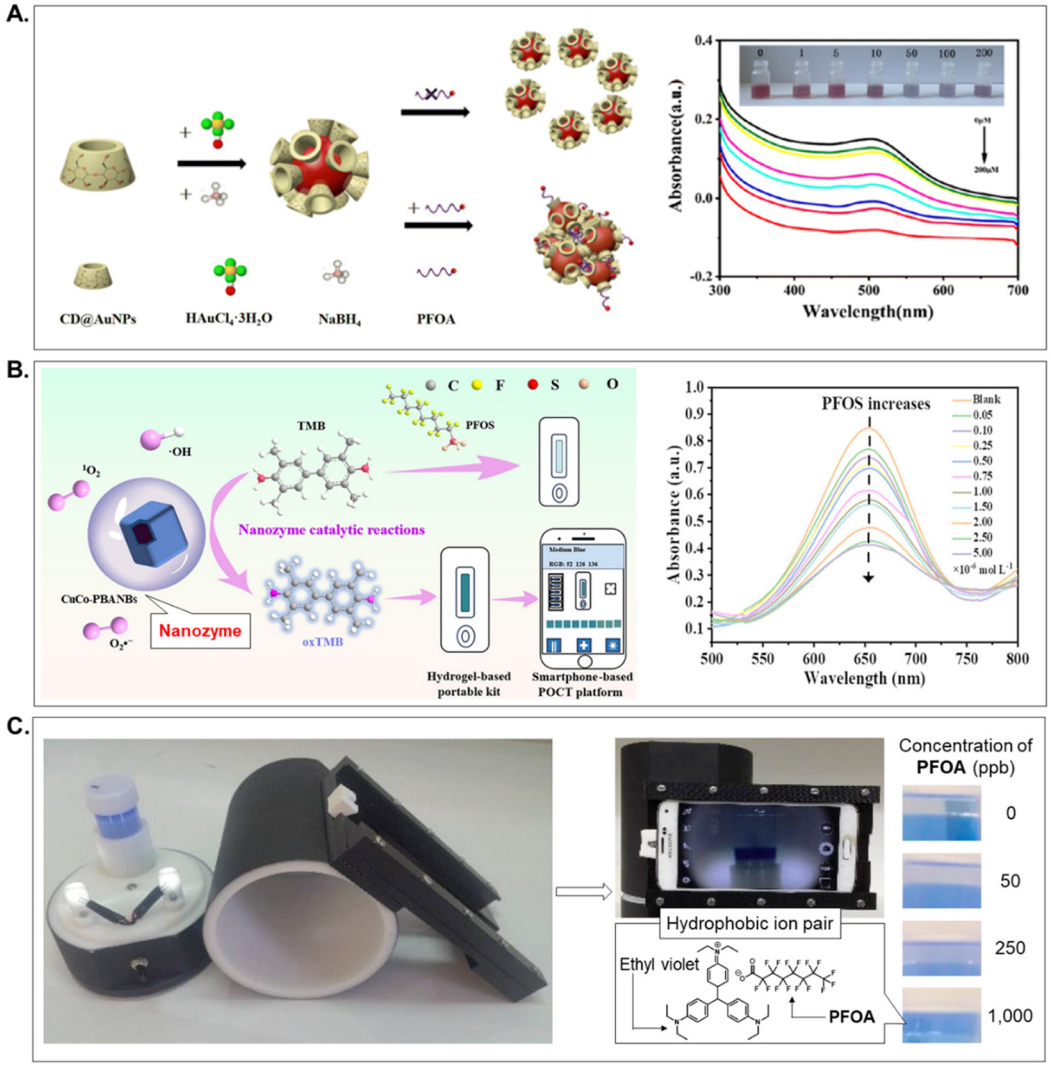

Fig. 3 Schematic of the colorimetric detection mechanism of specific PFASs: (A) aggregation induced by specific PFAS adsorption on Au NP surfaces; (B) inhibition of colouration resulting from specific PFAS adsorption onto the surface of nanozymes catalysing ROS generation; (C) monitoring the colour change of a solution containing hydrophobic ion pairs formed by dyes and specific PFASs using astkCARE™. Reproduced with permission from ref. 63, Copyright 2025 Royal Society of Chemistry; ref. 65, Copyright 2024 American Chemical Society; and ref. 80 Copyright 2018 Elsevier.

example reaction procedure is as follows: after incubating the nanozyme dispersion and PFAS aqueous solution for several tens of minutes, the mixture is treated with TMB solution, which is reactive to ROS. The treated solution is incubated for several tens of minutes, and its absorbance is measured at predetermined time points). These materials were affected by competitive adsorption involving some ions that easily coordinate with the terminal groups (*e.g.*, –COOH and $-SO_3H$) of specific PFASs, such as Cu^{2+} and SDS, as well as surfactants with structures similar to specific PFASs. Due to the involvement of ROSs generated on the nanozyme surface in detecting specific PFASs, further sensitivity improvements can be expected by performing SPE to remove contaminants such as ions and surfactants from these detection materials. Since the detection mechanism involves inhibiting ROS generation due to surface adsorption of PFASs onto the nanozyme, through surface modifications with substituents capable of altering interactions with different types of PFASs (*e.g.*, perfluoroalkyl chains with varying carbon chains lengths[76]), it is potentially possible to distinguish between different types and concentrations of PFASs under conditions where multiple PFASs coexist.

[3] Dye-based detection uses dyes that can interact with specific PFASs at the nano-level (*e.g.*, porphyrin derivatives with perfluoroalkyl chains that interact with PFASs *via* F–F interactions,[76–78] and methylene green that forms ion pairs with PFOS[79]). Among these, a portable kit called astkCARE™, which uses a dye (ethyl violet) similar to the active substance in methylene blue, is currently undergoing verification research with a view to practical application. This detection method involves extracting the hydrophobic ion pairs formed between ethyl violet and specific PFASs into an organic solvent

(*e.g.*, ethyl violet), enabling quantitative determination of the specific PFASs based on the colour change of the dye (Fig. 3C).[80,81] Additionally, the degree of colour change in the hydrophobic ion pairs formed by PFOA or PFOS and ethyl violet allows for the separate detection of PFOA and PFOS. In this method, without SPE, the formation of coordination bonds with inorganic anions (primary constituents in tap water: Cl^-, SO_4^{2-}, and others) was suggested, necessitating the removal of contaminants *via* SPE for enhanced sensitivity. However, astkCARE™ still involves several issues, including ppb-level LOD, the need for SPE to achieve a low LOD, the use of organic solvents that are generally non-disposable during the dissolution of materials responsible for detecting specific PFASs, and long detection time (approximately 3 h) that includes SPE. A porphyrin derivative,[76] featuring perfluoroalkyl chains with varying carbon chain lengths, has been reported to be able to control the type of PFAS susceptible to F–F interactions. This perfluoroalkyl chain has the following characteristics: (1) the hydrophobicity of the C–F bond site allows it to repel hydrocarbon contaminants such as dissolved organic matter.[82] (2) The low polarity and polarizability of the C–F bond site make it difficult to solvate ions, making it less susceptible to contaminants such as inorganic anions.[83] Therefore, optimizing the carbon chain length (hydrophobicity) of the perfluoroalkyl chain to match the carbon chain length of PFASs in aqueous environments enables the selective detection of different types of PFASs from aqueous environments containing contaminants. Based on (1) and (2), introducing perfluoroalkyl chains of various carbon chain lengths into dyes such as ethyl violet enables potential identification of the target PFASs in aqueous environments where multiple PFASs, dissolved organic matter, and inorganic anions coexist. In contrast, since most perfluoroalkyl chain-containing dyes are not water-soluble, PFASs cannot be detected directly in water; instead, detection and identification of PFASs must be performed in the organic solvent in which the dye is dissolved.

Based on [1]–[3], for practical application in on-site detection in actual aqueous environments, it is necessary to resolve issues such as the detection of specific PFASs at ppt levels, which is the regulatory value, the identification of the target PFASs in aqueous environments where multiple PFASs and contaminants exist based on differences in absorbance and absorption wavelength of detection materials, and the use of SPE and organic solvents.

2.2. Fluorescence detection

The detection of specific PFASs using fluorescent and quenching materials relies on changes in fluorescence intensity and wavelength that occur when the environment around the detection material changes owing to nano-level interactions with specific PFASs. These methods can be divided into three types: [1] 'turn-off type', in which the fluorescence intensity decreases upon the adsorption or binding of specific PFASs to the material surface; [2] 'turn-on type', in which the fluorescence intensity increases; and [3] 'ratiometric type', in which the fluorescence spectrum shifts upon specific PFAS binding. The detection performance of these materials relies on electron and energy transfer at the material surface, where specific PFASs are present. By optimizing the type of detection material and its interaction with specific PFASs, highly sensitive and selective detection of specific PFASs has been achieved, with a LOD at the ppt–ppb level.

[1] In 'turn-off type' detection, PFASs form aggregates by coordinating with the surface of the fluorescence material through electrostatic and hydrophobic interactions, causing aggregation-induced quenching (AIQ) (Fig. 4A).[84] Perylene-diimide-based fluorescent sensors (PDI-2+, Dalapati *et al.*[84]) and aggregation-induced conjugated polymers (FTD-MI, Zhao *et al.*[85]) quantitatively measure the AIQ of PFOA or PFOS by coordinating them to the surface of materials, respectively. Detection of specific PFASs (PFOA or PFOS, respectively) in these materials has achieved LODs of 0.32–1.9 ppb within approximately 1 min (without SPE) in water or in water/dimethyl sulfoxide (DMSO) mixed solution, with minimal influence of contaminants such as ions (*e.g.*, Na^+, K^+, and Cl^-) found in tap water and river water, and surfactants with structures similar to specific PFASs (*e.g.*, SDS and SDBS). Due to the evaluation of changes in fluorescence intensity at the same wavelength, these detection materials are expected to face difficulties in detecting and identifying each PFAS individually when multiple PFASs coexist. Furthermore, this method cannot completely eliminate the influence of background light from the detector during fluorescence measurements, making it necessary to exercise caution when interpreting small spectral changes.

[2] In 'turn-on type' materials, specific PFASs alter the electronic environment on the material surface, suppressing non-radiative quenching and increasing the fluorescence intensity of the detection material (Fig. 4B).[86] Dalapati *et al.* synthesized a Zr-MOF (U-1)[86] incorporating a hydrophobic perylene imide and a bifunctional MOF (UiO-66-N$(CH_3)^{3+}$).[87] In the case of U-1, the fluorescence intensity increased within 30 min (without SPE) in water or in water/organic solvent (DMSO or acetonitrile (MeCN)) mixed solution owing to the 'relaxation of π–π interactions *via* PFOA trapping within pores'. In contrast, UiO-66-N$(CH_3)^{3+}$ exhibited increased intensity *via* 'ion exchange between anionic dyes adsorbed on the material surface and PFOA', demonstrating a LOD of approximately 100–700 ppb. These materials were hardly affected by contaminants such as dissolved organic matter (*e.g.*, lauric acid) present in tap water or river water, or surfactants with structures similar to specific PFASs (*e.g.*, SDS and hexadecyltrimethylammonium bromide (CTAB)). Due to the evaluation of changes in fluorescence intensity at the same wavelength, these detection materials are expected to face difficulties in detecting and identifying each PFAS individually under the coexistence of multiple PFASs. Hassan *et al.* developed a hexanuclear cerium oxocluster ($[Ce_6(\mu_3\text{-}O)_4(\mu_3\text{-}OH)_4]^{12+}$) that exhibits aggregation-induced emission (AIE) upon interaction with PFAS and F–F bonds.[88] $[Ce_6(\mu_3\text{-}O)_4(\mu_3\text{-}OH)_4]^{12+}$ was able to effectively quantify low concentrations of PFOA (LOD: 0.24 ppb) and PFNA (LOD: 0.4 ppb) within 10 min (without SPE) in

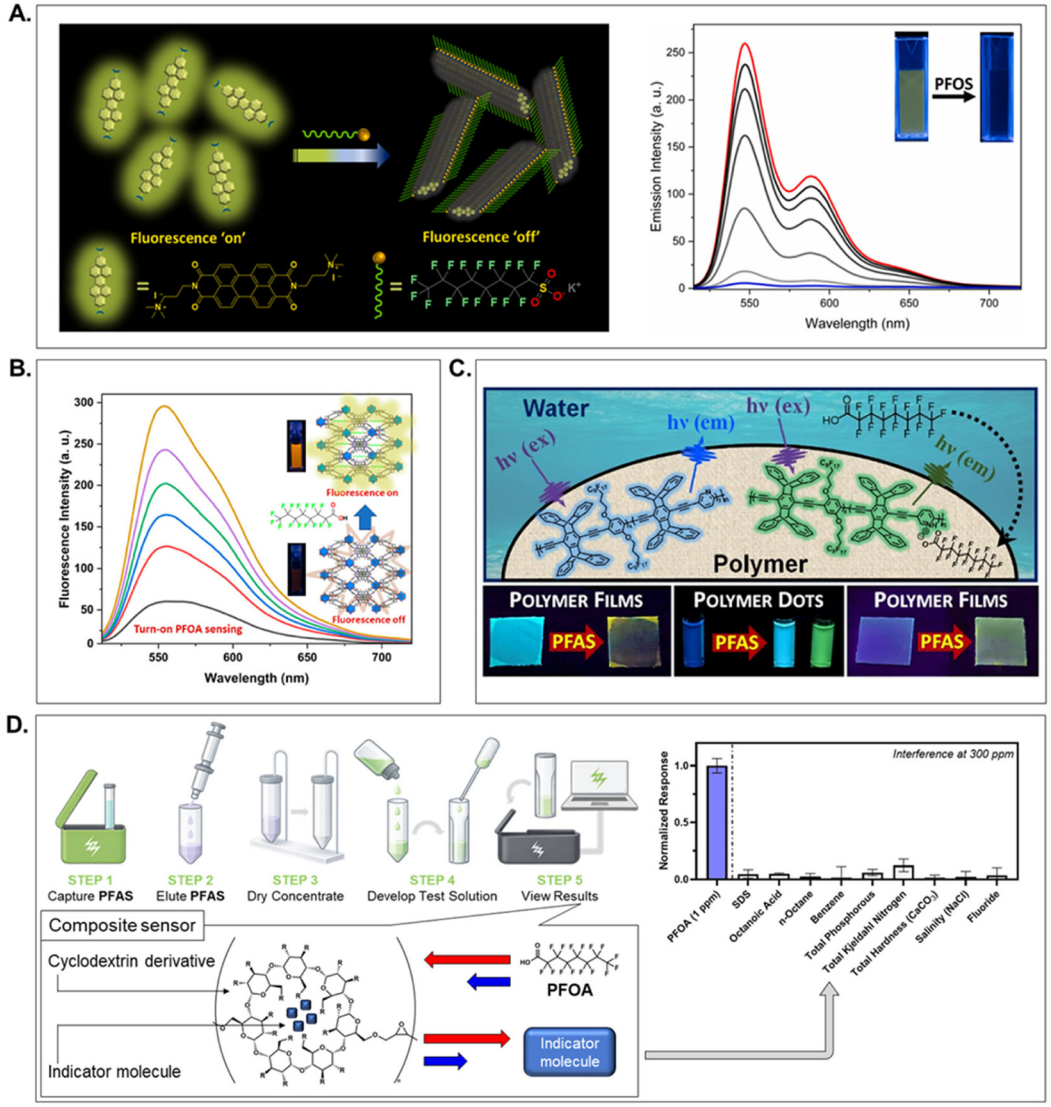

Fig. 4 Schematic of the fluorescence detection of specific PFASs: detection mechanism: (A) AIQ-induced quenching caused by specific PFAS coordination to the material surface (turn-off type); (B) fluorescence induced by changes in the electronic environment caused by specific PFAS coordination on the material surface (turn-on type); (C) change in fluorescence spectra owing to electron and energy transfer caused by specific PFAS coordination on the material surface (ratiometric type); and (D) fluorescence changes of a composite sensor including cyclodextrin and the indicator molecule with specific PFAS binding ability using FRED-PFAS™. Reproduced with permissions from ref. 84, Copyright 2025 Elsevier; ref. 86 and 92, Copyright 2023 and 2024 American Chemical Society; and ref. 59, Copyright 2025 National Ground Water Association.

water, and different types of PFASs such as PFHxA and PFDA could be distinguished from each other based on the change in fluorescence of the materials. This material was unaffected by ionic contaminants (*e.g.*, Na^+, K^+, and Cl^-) found in tap water and river water. Xu *et al.* synthesized a Tb(III) coordination polymer ($\{Tb(L)(NO_3)(H_2O)_2\}_n$) that displays AIE upon electrostatic interaction with specific PFASs, achieving PFOA detection at ultra-low concentrations within 10 min (without SPE) in water (LOD: 27.3 ppt) and is unaffected by interfering ions or surfactants.[89] $\{Tb(L)(NO_3)(H_2O)_2\}_n$ was unaffected by contaminants such as ions (*e.g.*, Na^+, K^+, and Cl^-) present in tap water or river water, or surfactants (*e.g.*, SDS and SDBS) with structures similar to specific PFASs. Due to the evaluation of changes in fluorescence intensity at the same wavelength, these detection materials are also expected to face difficulties in detecting and identifying each PFAS individually in the presence of multiple PFASs. A composite (SA hydrogel-N,F-CD composite) formed by encapsulating fluorinated carbon dots (F-CD) in an alginate hydrogel increased the luminescence quantum yield by confining PFOA within the nanoscale space *via* F–F interactions between F-CD and PFOA. Although this system was noted to achieve ultra-high-sensitivity detection within 1 h (without SPE) in water (LOD: 0.001 ppt), it also exhibited slight fluorescence due to F–F interactions with contaminant (NaF).[90,91] The detection mechanism of this composite relies on F–F interactions with PFASs in the nanoscale

space, enabling enhanced selectivity for specific PFAS detection through removal of contaminants (NaF) using SPE. Similar to other 'turn-off type' detection materials, all detection materials for 'turn-on type' are expected to have difficulty detecting and identifying individual PFASs in the presence of multiple PFASs, as they evaluate changes in fluorescence intensity at a single wavelength.

[3] The 'ratiometric type' quantifies specific PFASs by analysing the intensity ratio of fluorescence wavelengths before and after the specific PFASs interact with the detection material, offering improved performance in complex aqueous environments (Fig. 4C).[92] Lanthanide MOF-based surface molecularly imprinted polymer probes (Eu/Tb-MOF@MIPs, Yang *et al.*[93]) were noted to amplify fluorescent polymers (PPE-Py*, Concellón *et al.*[92]), and probes combining molybdenum boride (MoB) quantum dots (QDs) with N,F-CD (MoB QD/N,F-CD, Wang *et al.*[94]) enabled PFOA detection in water (without SPE) (LOD: 0.1–40.6 ppb). Some materials were affected by ions (*e.g.*, Fe^{2+} and Fe^{3+}) that readily coordinate with the terminal functional groups of specific PFASs. Due to the interaction between the surfaces of the material and specific PFASs being involved in the detection mechanism, the selectivity for detecting specific PFASs is expected to improve by removing contaminants using SPE. Based on the intensity ratio of different fluorescence wavelengths, these materials may enable the detection and identification of PFAS types and concentrations in the presence of multiple PFASs. These methods primarily relied on changes in the ratio of two fluorescence intensities induced by binding to PFOA *via* F–F and electrostatic interactions. Donor–acceptor conjugated polymers (PF-DBT-Im, Chen *et al.*[95]) and aggregation-induced conjugated polymers (FTD-C8-MI, Zhao *et al.*[85]) incorporate structures exhibiting both fluorescence resonance energy transfer (FRET) and AIE within the same backbone. These detection materials enable the quantification of PFOA and PFOS present in water at the ppb level within several minutes (without SPE) based on the change in fluorescence by altering FRET through electrostatic or hydrophobic interactions with specific PFASs (LOD: 0.32–7.15 ppb). Several materials[94,95] are affected by contaminants (*e.g.*, SO_4^{2-}, NO_3^-, Cl^-, hydroquinone (HQUI), SDS, and SDBS) that promote the aggregation of detection materials involved in the fluorescence energy transfer through electrostatic, hydrophobic, and π–π interactions. By improving the dispersion stability of the detection material using surfactants that are structurally dissimilar to PFASs (and do not impair interactions with PFASs), it is considered possible to prevent the aggregation of the detection material caused by contaminants. Similar to other 'ratiometric' detection materials, based on the intensity ratio of different fluorescence wavelengths for the detection of PFASs, this method enables the detection and identification of PFAS species and concentrations even in the presence of multiple PFASs.

In terms of on-site detection of PFASs using fluorescent materials, the verification research of FRED-PFAS™, a composite sensor consisting of a CD derivative capable of binding to specific PFASs and an indicator molecule (dye), is underway (Fig. 4D).[59,96,97] The portable FRED-PFAS™ can detect PFOA at the ppb–ppm level in organic solvents (methanol) and showed no response to Cl^-, CO_3^{2-}, or surfactants like SDS, although it faces several challenges, such as insufficient performance at the ppt level, undifferentiable from PFASs (fluorotelomers and aqueous film-forming foam) other than PFOA, the need for SPE to achieve a low LOD, the use of methanol that is generally non-disposable during the dissolution of materials responsible for detecting specific PFASs, and a long detection time (approximately 4 h) that includes SPE. Additionally, since FRED-PFAS™ is a detection technology based on changes in fluorescence intensity at the same wavelength, it is expected to be difficult to distinguish the target PFASs from aqueous environments where multiple PFASs coexist.

Considering these findings, on-site detection of specific PFASs in actual aqueous environments requires overcoming challenges such as detection of specific PFAS at ppt levels in water containing contaminants, identification of the target PFASs in water containing multiple PFASs and contaminants due to differences in the fluorescence intensity and wavelength of the detection material, and the use of SPE and organic solvents.

2.3. Electrochemical detection

PFASs are electrochemically inactive and cannot be oxidized or reduced. Therefore, direct electrochemical detection of specific PFASs is generally not possible, and indirect strategies that enhance sensitivity are required. These approaches promote nano-level interfacial reactions between the electrode surface and specific PFAS to detect the target substance as an electrical signal. Representative technologies include [1] fabrication of electrodes incorporating nanostructures that can interact with specific PFASs, and [2] nanosized template synthesis of specific PFASs on the electrode surface. By improving the electron-transfer properties of the electrode surface and adsorption of specific PFASs at the interface, high-sensitivity electrochemical detection at the ppt–ppb level can be realized. On the other hand, for stable specific PFAS detection, a supporting electrolyte such as phosphate-buffered saline (PBS) must be used in all electrochemical measurements.

[1] In the context of nanostructured electrodes, Shanbhag *et al.* fabricated a graphene-based electrode (G/CPE) with high adsorption capacity for specific PFASs owing to its high specific surface area.[98] G/CPE can quantify changes in electrical signals resulting from interactions between graphene π-electrons and specific PFASs, and was able to instantly detect PFOA (LOD: 4.31 ppb) and PFDA (LOD: 8.53 ppb) using PBS as the supporting electrolyte (without SPE). Nevertheless, this detection material was noted to be reactive toward contaminants, such as Zn^{2+}, Ni^{2+}, and HQUI, which are likely to compete for adsorption through interactions similar to those of PFASs (*e.g.*, electrostatic and hydrophobic interactions). To this end, removal of contaminants using SPE is recommended prior to detecting specific PFASs. Since this electrode cannot identify interactions based on the slight structural differences between various PFASs, detecting and identifying each PFAS in

the presence of multiple PFASs is expected to be difficult. Au NPs,[99–101] silver nanoparticles (Ag NPs),[102] and copper-incorporated nanostructures (F-Cu-NH_2BDC, Zheng *et al.*;[103] Cu@CuO aerogel, Xu *et al.*[104]) with excellent electron transfer properties have been used for highly sensitive detection of PFASs (Fig. 5A).[103] In general, the surfaces of Au NPs or Ag NPs can be functionalized with substances capable of interacting with specific PFASs, such as dyes (MB@AuNPs, Simonetti *et al.*[99]), perfluoroalkyl chains (carbon chain length of 8 or more) (PFTD/AuNPs/GCE, Calvillo Solís *et al.*[100]), citrate (MXene-AgNPs[102]), and nickel oxide (AuNPs/NiOScZ/SPCE, Comnea-Stancu *et al.*[101]). These materials were able to quantify trace amounts of PFASs (perfluorobutanoic acid (PFBA), PFOA, PFOS, perfluoroundecanoic acid (PFUnDA), each a single substance) within 1 h using PBS or $KHCO_3$ as the supporting electrolyte (without SPE) (LOD: 0.033–24.0 ppt). However, it was revealed that electrochemical reactivity toward contaminants such as Mg^{2+} and Na^+, which readily coordinate with the terminal functional groups of specific PFASs, as well as SDS and SDBS, which have structures similar to specific PFASs, and that the selectivity for PFAS detection was low. In the detection technologies described in [1], while these materials have the advantage of detecting ppt-level specific PFASs through electrostatic interactions or hydrophobic interactions between the electrode and the specific PFAS, the interaction between the material surface and the specific PFAS significantly influences the detection mechanism; consequently, they are susceptible to interference from inorganic anions and surfactants, and have the limitation necessitating the contaminant removal step using SPE. These materials, by surface-modifying substances with varying abilities to interact with various PFASs (*e.g.*, perfluoroalkyl chains with varying carbon chain lengths

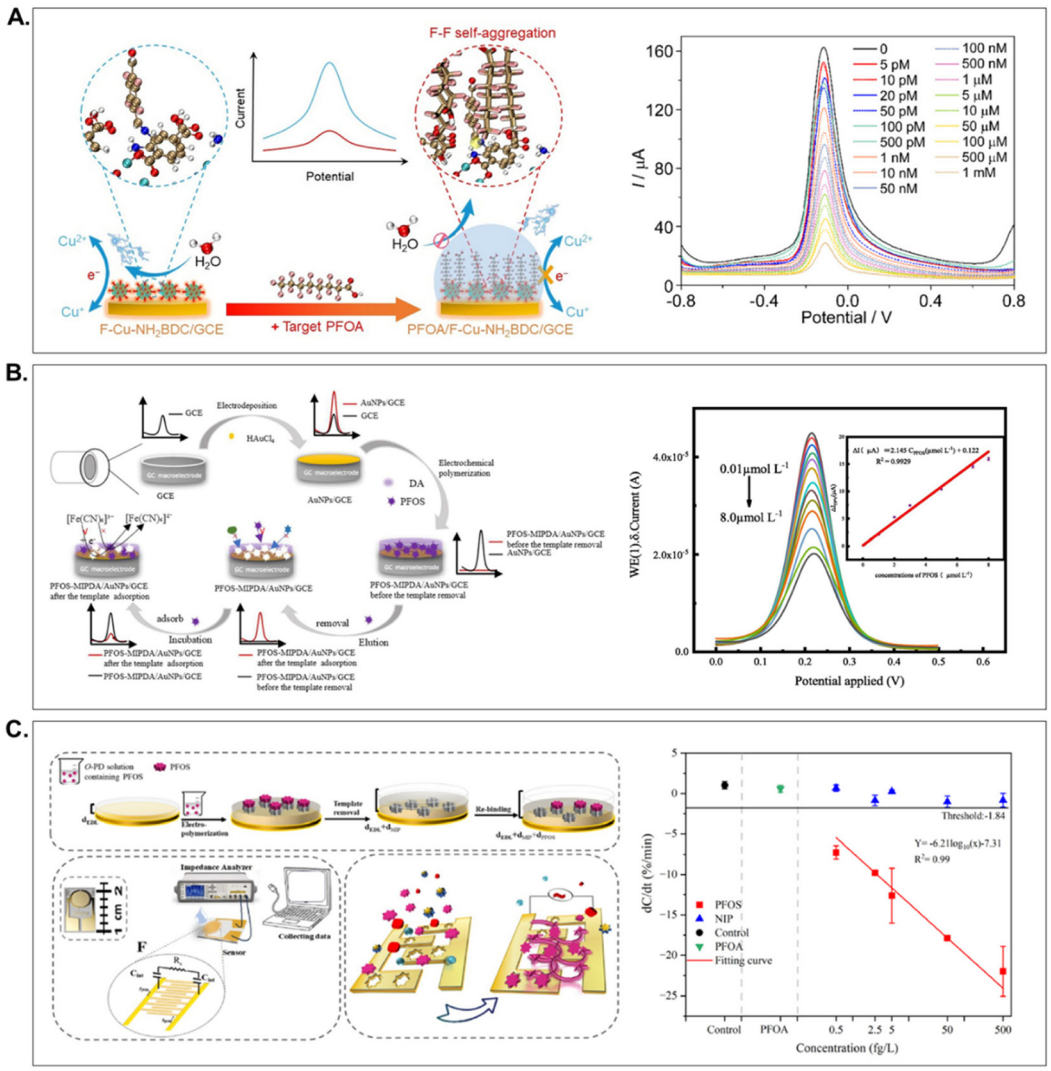

Fig. 5 Schematic of the electrochemical detection of specific PFASs: detection mechanism: adsorption of specific PFASs onto nanosized templates prepared on the electrode surface by the electrolytic polymerization of (A) dopamine or (B) *o*-phenylenediamine; (C) electrical signal enhancement using electrodes incorporating substances capable of interacting with specific PFASs. Reproduced with permissions from ref. 103 and 105, Copyright 2023 Elsevier; and ref. 106, Copyright 2025 American Chemical Society.

(3–12)),[76] may enable detection and identification tailored to the type and concentration of PFASs even in the presence of multiple PFASs.

[2] In nanosized template synthesis, electrolytic polymerization of dopamine or *o*-phenylenediamine occurs on the electrode surface in the presence of PFOS (Fig. 5B and C).[105–108] The binding of PFOS to the nanosized template can be detected as a change in electrical signal. Sensors fabricated by Amin *et al.* (molecularly imprinted poly *o*-PD on Au interdigitated microelectrodes)[106] and Lu *et al.* (MIP/AuNS/GCE)[108] achieved ppt-level LODs within minutes (without SPE). Some of these materials demonstrate high detection sensitivity for PFOS among PFAS species (perfluoropentanoic acid (PFPA), perfluoroheptanoic acid (PFHpA), and PFOA, each as a single substance) under conditions using PBS as the supporting electrolyte. Nevertheless, sensitivity to some contaminants such as Na^+, Cl^-, and humic acid, which are likely to competitively adsorb to the electrode surface through similar interactions (*e.g.*, electrostatic and hydrophobic interactions) to PFASs, has been reported.[108] The methods used to enhance the detection sensitivity and selectivity of this electrode for specific PFASs include removing contaminants *via* SPE and surface modification of the electrode using substituents that readily interact with PFASs. In the detection technologies described in [2], these materials have the advantage of controlling the detection sensitivity for PFOS and other PFASs through nanosized templates fabricated on the electrode surface using PFOS. On the other hand, the nanosized template synthesis for different types of PFASs (especially those with short carbon chains) is challenging (due to weak interactions between the monomers used in electrolytic polymerization and PFASs with short carbon chains), and they are susceptible to competitive adsorption with inorganic anions and surfactants on the material surface, and have the limitation necessitating a process for removing contaminants using SPE. Therefore, by applying the methods described in [1] (incorporation of nanostructures and surface modification of substituents that easily interact with PFASs) to electrodes equipped with nanosized templates, it is potentially possible to distinguish between different types and concentrations of PFASs in the presence of multiple PFASs without SPE.

As described in [1] and [2], to apply this technology to on-site detection in actual aqueous environments, it is necessary to resolve issues such as installation of equipment for electrochemical detection in a wide area (ensuring a stable power source and preparing the optimal supporting electrolyte for each water body), selective detection of PFAS in the presence of contaminants, and identification of the target PFASs in aqueous environments where multiple PFASs exist due to differences in potential.

2.4. SERS detection

SERS is a powerful spectroscopic technology capable of detecting molecule-specific vibrational spectra. For ultra-low concentration analysis of specific PFASs using SERS, the selection of a substrate capable of enhancing Raman signals and the immobilization of specific PFASs onto the substrate are critical. Typically, substrates are coated with Ag NPs that provide electromagnetic enhancement *via* localized surface plasmon resonance. To detect changes in Raman signals based on the presence of specific PFASs on the substrate, two approaches have been designed: [1] sandwiching specific PFASs between Ag NPs and Au NPs, and [2] adding or modifying materials to the Ag NP surface to facilitate specific PFAS immobilization.

[1] Feng *et al.* deposited a mixture of Ag NPs and PFASs onto a substrate containing Au NPs, allowing the PFAS to be sandwiched between the Ag NPs and Au NPs after drying (Fig. 6A).[109] This sandwich method enabled the identification of PFHxA, PFOA, and PFBS in water based on slight differences in the Raman signal peak positions, with a LOD value of 100 ppb for each (without SPE). The effect assessment of contaminants on this method had been untested. Identification of PFAS using this method relies on slight differences in the peak positions of Raman signals originating from structurally similar types of PFASs; hence, in the presence of multiple PFASs, peak position shifts are expected to occur competitively in principle, making detection and identification based on PFAS types and concentrations difficult.

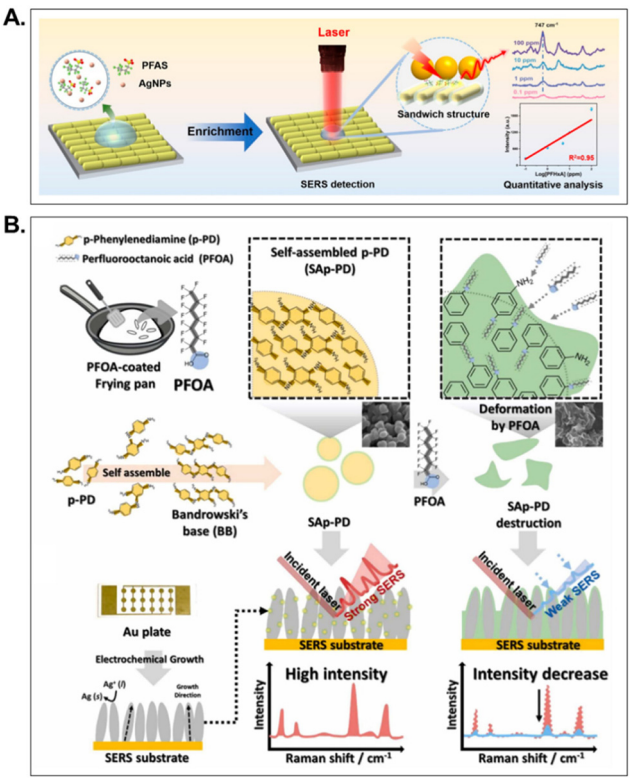

Fig. 6 Schematic of the SERS detection of specific PFASs: detection mechanism: (A) enhancement of the Raman signal by sandwiching specific PFASs with Au NPs and Ag NPs, (B) enhancement of the Raman signal using Ag NPs modified with substances capable of interacting with specific PFASs. Reproduced with permissions from ref. 109, Copyright 2023 American Chemical Society; and ref. 111, Copyright 2023 Elsevier.

Table 1 Summary table of **PFAS** detection by colorimetric technology. Interfering species of each research were excerpted from representative ions, surfactants, and dissolved organic matter, among others

Detection method	Material	Analyte	LOD	Detection time	Measurement solvent	Interfering species	Selectivity	Detection mechanism	Ref.
Colorimetric	**CD@AuNPs**	**PFOA**	70.4 ppb	60 min	Water/DMF	Environmental water samples	Good	Aggregation due to **PFAS** adsorption on the surface of **Au NPs**	63
	Citrate-Au NPs	**PFHxA** **PFOA** **PFNA** **PFDA** **PFOS** **PFOPA**	42.7–2005 ppb	1 s	Water	Cl^-, Na^+, Mg^{2+}, Suwanee river dissolved organic matter, and pH (4, 7, and 10)	Affected by dissolved organic matter, ions (Cl^- and Mg^{2+}), and pH (7 and 10)	Inhibition of color reaction resulting from **PFAS** adsorption on the surface of the nanozyme catalyzing ROS generation	64
	CuCo-PBA NB	**PFOS**	7.15 ppb	30 min	Water	NO_3^-, SO_4^{2-}, CO_3^{2-}, Ac^-, HCO_3^-, HPO_4^{2-}, Ni^{2+}, Na^+, Al^{3+}, Cu^{2+}, Ba^{2+}, Fe^{2+}, Fe^{3+}, SDS, CTAB, and PVP	Affected by ions (CO_3^{2-}, HCO^{3-}, Ba^{2+}), surfactants (SDS, CTAB, PVP)		65
	Fe_3O_4@MON-F@Ru	**PFOS**	7.70 ppb	50 min	MeOH	Cl^-, NO_3^-, SO_4^{2-}, Na^+, K^+, and Fe^{2+}	Good		66
	F-Ce-UiO-66-NH_2	**PFOA**	169.8 ppb	40 min	Water	F^-, Cl^-, Br^-, NO_3^-, SO_4^{2-}, Na^+, K^+, Mg^{2+}, Cu^{2+}, Fe^{3+}, Zn^{2+}, Cr^{3+}, Pb^{2+}, NH_4^+, SDBS, and PVP	Good		67
	Fe/Zn-BDC	**PFOS**	50.0 ppb	15 min	Water	F^-, Cl^-, Br^-, SO_4^{2-}, CO_3^{2-}, Na^+, K^+, Mg^{2+}, Ca^{2+}, PVP, CTAB, and CTAC	Good		68
	MOFs derived Cu/C nanocomposite	**PFOA**	55.1 ppb	40 min	Water	Cl^-, SO_4^{2-}, HPO_4^{2-}, Ac^-, Cu^{2+}, Fe^{3+}, Na^+, and SDS	Good		69
	PCN-222(Fe)-3F	**PFOS**	6.30 ppb	30 min	Water	Cl^-, SO_4^{2-}, CO_3^{2-}, HPO_4^{2-}, Ac^-, Na^+, K^+, Mg^{2+}, Ca^{2+}, Cu^{2+}, SDS, SOS, and CTAB	Affected by surfactants (SDS, SOS, and CTAB)		70
	MGO@ZIF-8@MIP	**PFOA**	49.7 ppb	50 min	Water	Na^+, K^+, and Mg^{2+}	Good		71
	$[(CH_3)_2NH_2]V_3O_7$	**PFOS**	230.0 ppb	20 min	Water	Cl^-, Br^-, SO_4^{2-}, CO_3^{2-}, HPO_4^{2-}, Na^+, K^+, Mg^{2+}, Ca^{2+}, Zn^{2+}, Ni^{2+}, Mn^{2+}, SDS, CTAB, PVP, and CTAC	Good		72
	AuNCs@CMP	**PFOS**	75.0 ppb	20 min	Water	Cl^-, SO_4^{2-}, Na^+, K^+, and Mg^{2+}	Good		73
	SMIP@N-CF	**PFOA**	401.7 ppb	5 min	Water	—	Untested		74
	Cu-CN	**PFOS**	7.45 ppb	30 min	Water	SO_4^{2-}, CO_3^{2-}, $B_4O_7^{2-}$, HPO_4^{2-}, $H_2PO_4^-$, Ac^-, Na^+, Ca^{2+}, Cu^{2+}, Fe^{3+}, Fe^{2+}, SDS, SDBS, SOS, CTAB, and PVP	Affected by surfactants (SDS)		75
	astkCARE™	**PFOA**	10 ppb (without **SPE**)	5 min (without **SPE**)	Water/EtOAc	Tap water and ground water	Affected by inorganic ions in tap/ground water	Color change of a solution containing hydrophobic ion pairs formed by dyes and **PFASs**	80
		PFOS	0.5 ppb (with **SPE**)	3 h (with **SPE**)					81

Abbreviations: **PFHxA**: perfluorohexanoic acid; **PFOA**: perfluorooctanoic acid; **PFNA**: perfluorononanoic acid; **PFDA**: perfluorodecanoic acid; **PFOS**: perfluorooctanesulfonic acid; **PFOPA**: 1*H*,1*H*,2*H*,2*H*-perfluorooctanephosphonic acid; **SPE**: solid-phase extraction; DMF: *N*,*N*-dimethylformamide; MeOH: methanol; EtOAc: ethyl acetate; SDS: sodium dodecyl sulfate; SDBS: sodium dodecylbenzene sulfonate; SOS: sodium octyl sulfate; CTAB: cetyltrimethylammonium bromide; CTAC: cetyltrimethylammonium chloride; and PVP: polyvinylpyrrolidone. "—" indicates that the "**Selectivity**" column was "Untested". "Good" in the "**Selectivity**" column indicates that the detection material did not show significant changes in the interfering species tested in that research.

Table 2 Summary table of **PFAS** detection by fluorescence technology. Interfering species of each research were excerpted from representative ions, surfactants, and dissolved organic matter, among others

Detection method	Material	Analytes	LOD	Detection time	Measurement solvent	Interfering species	Selectivity	Detection mechanism	Ref.
Fluorescence	**PDI-2+**	**PFOS**	1.9 ppb	1 min	Water	NO_3^-, HCO_3^-, $S_2O_3^{2-}$, PO_4^{3-}, Na^+, K^+, Mg^{2+}, Ca^{2+}, Fe^{3+}, Li^+, SDS, lauryl sulfate, and lauric acid	Good	AIQ-induced quenching caused by **PFAS** coordination to the material surface (turn-off type)	84
	FTD-MI, FTD-C_8-MI		**FTD-MI**: 1.18 ppb (**PFOA**)	1 s	Water/DMSO	Cl^-, NO_3^-, SO_4^{2-}, CO_3^{2-}, HPO_4^{2-}, HSO_3^- Ac^-, Na^+, Cu^{2+}, Fe^{3+}, Mn^{2+}, Pb^{2+}, Bi^{3+}, Co^{2+}, Cd^{2+}, Ce^{2+}, CTAB, and CTAC	Good		85
		PFOA	0.32 ppb (**PFOS**)						
		PFOS	**FTD-C_8-MI**: 2.24 ppb (**PFOA**) 2.42 ppb (**PFOS**)						
	U-1	**PFOA**	695.6 ppb	30 min	Water/DMF	CTAB and lauric acid	Good	Fluorescence due to changes in the electronic environment caused by **PFAS** coordination on the material surface (turn-on type)	86
	UiO-66-N$(CH_3)^{3+}$	**PFOA**	91.1 ppb	40 min	Water/MeCN	SDS and lauric acid	Good		87
	$[Ce_6(\mu_3\text{-}O)_4(\mu_3\text{-}OH)_4]^{12+}$	**PFHxA**		10 min	Water	F^-, Cl^-, I^-, CO_3^{2-}, PO_4^{3-}, Na^+, and K^+	Good		88
		PFOA	0.24 ppb (**PFOA**)						
		PFNA	0.4 ppb (**PFNA**)						
		PFDA							
	{Tb(L)$(NO_3)(H_2O)_2$}vv$_n$	**PFOA**	27.3 ppt	10 min	Water	F^-, Cl^-, NO_3^-, SO_4^{2-}, SCN^-, Na^+, Mg^{2+}, Fe^{2+}, NH_4^+, SDS, SDBS, and CTAB	Good		89
	SA hydrogel-N, F-CDs composite	**PFOA**	0.001 ppt	60 min	Water	Cl^-, NO_3^-, $H_2PO_4^-$, Na^+, K^+, Ca^{2+}, and Ni^{2+}	Good		90
	F-CD	**PFOA**	3.0 ppt	30 min	Water/EtOH	F^-, Cl^-, NO_3^-, HPO_4^{2-}, $H_2PO_4^-$, Na^+, K^+, Ca^{2+}, Fe^{3+}, and Ni^{2+}	Affected by ions (F^-)		91
	PPE-Py*	**PFOA**	100 ppt	60 min	Water	—	Untested	Change in fluorescence spectra due to electron and energy transfer caused by **PFAS** coordination on the material surface (ratiometric type)	92
	Eu/Tb-MOF@MIPs	**PFOA**	40.6 ppb	4 min	Water	F^-, Cl^-, NO_3^-, CO_3^{2-}, Na^+, K^+, Mg^{2+}, and Ca^{2+}	Good		93
	MoB QDs and N, F-CDs	**PFOA**	4.14 ppb	4 min	Water	Cl^-, Br^-, NO_3^-, SO_4^{2-}, CO_3^{2-}, Na^+, K^+, Mg^{2+}, Cu^{2+}, Fe^{2+}, Fe^{3+}, Zn^{2+}, Mn^{2+}, Ba^{2+}, Al^{3+}, Cr^{3+}, NH^4, and CTAB	Affected by ions (Br^-, Fe^{2+}, Fe^{3+}, Al^{3+}, and Cr^{3+}) and surfactants (CTAB)		94
	PF-DBT-Im	**PFOA**	2.53 ppb (**PFOA**)	1 s	Water	Cl^-, I^-, SO_4^{2-}, CO_3^{2-}, Ac^-, $H_2PO_4^-$, Na^+, Mg^{2+}, Ca^{2+}, Cu^{2+}, Ba^{2+}, Fe^{2+}, Fe^{3+}, Zn^{2+}, Cr^{3+}, Co^{2+}, Ni^{2+}, Ag^+, Cd^{2+}, Pb^{2+}, Ce^{2+}, SDS, SDBS, CTAB, CTAC, Tween-20, and PEG-4000	Affected by surfactants (SDS and SDBS)		95
		PFOS	7.15 ppb (**PFOS**)						
	FRED-PFAS™	**PFOA** **6 : 2 FTS AFFF**	1 ppm (**PFOA**)	4 h (with **SPE**)	Water/MeOH	Cl^-, CO_3^{2-}, Na+, Ca^{2+}, and SDS	Good	Fluorescence changes of the composite sensor of cyclodextrin and the indicator molecule with **PFAS** binding ability	59 96 97

Abbreviations: **PFHxA**: perfluorohexanoic acid; **PFOA**: perfluorooctanoic acid; **PFNA**: perfluorononanoic acid; **PFDA**: perfluorodecanoic acid; **PFOS**: perfluorooctanesulfonic acid; **6 : 2 FTS**: 6 : 2 fluorotelomer sulfonate; **AFFF**: aqueous film-forming foam; **SPE**: solid-phase extraction; DMF: *N*,*N*-dimethylformamide; MeOH: methanol; DMSO: dimethyl sulfoxide; MeCN: acetonitrile; EtOH: ethanol; SDS: sodium dodecyl sulfate; SDBS: sodium dodecylbenzene sulfonate; CTAB: cetyltrimethylammonium bromide; CTAC: cetyltrimethylammonium chloride; Tween-20: polyoxyethylene (20) sorbitan monolaurate; and PEG-4000: polyethylene glycol 4000. "—" indicates that the "**Selectivity**" column was "Untested". "Good" in the "**Selectivity**" column indicates that the detection material did not show significant changes in the interfering species tested in that research.

Table 3 Summary table of **PFAS** detection by electrochemical technology. Interfering species of each research were excerpted from representative ions, surfactants, and dissolved organic matter, among others

Detection method	Material	Analytes	LOD	Detection time	Measurement solvent	Interfering species	Selectivity	Detection mechanism	Ref.
Electrochemical	**G/CPE**	**PFOA** **PFDA**	4.31 ppb (**PFOA**) 8.53 ppb (**PFDA**)	1 s	PBS/EtOH	Cl^-, NO_3^-, SO_4^{2-}, CO_3^{2-}, Na^+, K^+, Mg^{2+}, Cu^{2+}, Fe^{2+}, Zn^{2+}, and Ni^{2+}	Affected by ions (Cl^-, NO_3^-, SO_4^{2-}, K^+, Mg^{2+}, Fe^{2+}, and Ni^{2+})	Electrical signal enhancement using electrodes incorporating substances capable of interacting with **PFASs**	98
	MB@AuNPs	**PFBA** **PFUnDA** **PFOS**	2.7 ppt	150 s	PBS	Na^+, Ca^{2+}, SDS, CTAB, and Tween-20	Affected by surfactants (SDS)		99
	PFTD/AuNPs/GCE	**PFOA**	24 ppt	120 s	$KHCO_3$ solution	—	Untested		100
	AuNPs/NiOScZ/SPCE	**PFOA**	12 ppt	1 s	PBS	NO_3^-, Na^+, K^+, Ca^{2+}, Cu^{2+}, Fe^{2+}, Mn^{2+}, and HQUI	Good		101
	MXene-AgNPs	**PFOS**	0.033 ppt	5 min	PBS	F^-, Cl^-, I^-, SO_4^{2-}, PO_4^{3-}, Na^+, K^+, Mg^{2+}, and 4-DBS	Affected by surfactants (4-DBS)		102
	F-Cu-NH_2BDC	**PFOA**	1.47 ppt	1 s	PBS	Na^+, K^+, Mg^{2+}, Cu^{2+}, Fe^{3+}, Zn^{2+}, Pb^{2+}, Co^{2+}, Cr^{3+}, Ni^{2+}, SDS, SDBS, and CTAB	Good		103
	Cu@CuO aerogel	**PFOS**	1.65 ppb	30 min	PBS	Na^+, K^+, Mg^{2+}, Ca^{2+}, Mn^{2+}, Cd^{2+}, Ce^{2+}, SDS, SDBS, and PVP	Affected by ions (Mn^{2+}), surfactants (SDS, SDBS, and PVP)		104
	PFOS-MIPPDA/AuNPs/GCE	**PFOS**	2.1 ppb	15 min	PBS	Cl^-, SO_4^{2-}, CO_3^{2-}, SiO_3^{2-}, Na^+, K^+, Mg^{2+}, Ca^{2+}, Ba^{2+}, and NH_4^+	Good	Adsorption of **PFASs** onto nanosized templates prepared on the electrode surface	105
	Molecularly imprinted poly *o*-PD preparation on Au-IDMEs	**PFPA** **PFHpA** **PFOA** **PFOS**	0.0005 ppt (**PFOS**)	10 s	PBS	—	Untested		106
	CNW/MIP	**PFOS**	1.2 ppb	12 min	PBS	—	Untested		107
	MIP/AuNS/GCE	**PFOS**	7.5 ppt	10 min	PBS/MeOH	Cl^-, Na^+, and humic acid	Affected by ions (Cl^-)		108

Abbreviations: **PFBA**: perfluorobutanoic acid; **PFPA**: perfluoropentanoic acid; **PFHpA**: perfluoroheptanoic acid; **PFOA**: perfluorooctanoic acid; **PFUnDA**: perfluoroundecanoic acid; PBS: phosphate buffered saline; MeOH: methanol; EtOH: ethanol; SDS: sodium dodecyl sulfate; SDBS: sodium dodecylbenzene sulfonate; CTAB: cetyltrimethylammonium bromide; PVP: polyvinylpyrrolidone; HQUI: hydroquinone; and 4-DBS: 4-dodecylbenzenesulfonic acid. "—" indicates that the "**Selectivity**" column was "Untested". "Good" in the "**Selectivity**" column indicates that the detection material did not show significant changes in the interfering species tested in that research.

Table 4 Summary table of **PFAS** detection by **SERS** technology. Interfering species of each research were excerpted from representative ions, surfactants, and dissolved organic matter, among others

Detection method	Material	Analytes	LOD	Detection time	Measurement solvent	Interfering species	Selectivity	Detection mechanism	Ref.
SERS	**Au@AgNRs**	**PFHxA PFOA PFBS**	100 ppb	1 s	Water	—	Untested	Enhancement of the Raman signal by sandwiching **PFASs** with **Au NPs** and **Ag NPs**	109
	AgNPs on fish scale substrates	**PFOS**	49.1 ppb	1 s	Water	Lake water, soil, and urine samples	Good	Enhancement of the Raman signal using **Ag NPs** modified with substances	110
	Self-assembled *p*-phenylenediamine (SAp-PD) nanoparticles	**PFOA**	0.53 ppt	1 s	Water	Tap water, oxalic acid, citric acid, and succinic acid	Good	capable of interacting with **PFASs**	111
	AgNR substrate	**PFOA**	1 ppt (**PFOA**)	1 s	MeOH	—	Untested		112
		PFOS	4.28 ppb (**PFOS**)						
	Graphene and Ag NPs printed on a kapton substrate	**PFOA PFOS**	0.40 ppt	1 s	Water	—	Untested		113
	β-CD/Ag nanocomplexes in the microstructured optical fiber	**PFOA**	40 ppt	1 s	Water	—	Untested		114

Abbreviations: **PFHxA**: perfluorohexanoic acid; **PFOA**: perfluorooctanoic acid; **PFBS**: perfluorobutanesulfonic acid; **PFOS**: perfluorooctanesulfonic acid; and MeOH: methanol. "—" indicates that the "**Selectivity**" column was "Untested". "Good" in the "**Selectivity**" column indicates that the detection material did not show significant changes in the interfering species tested in that research.

[2] Kumar *et al.* added malachite green, which forms ion pairs with specific PFASs, to increase the affinity between Ag NPs on a substrate and specific PFASs.[110] This method enabled the rapid quantification of PFOS in water, with a LOD of 49.1 ppb. In addition, there was no effect from contaminants contained in soil and lake water, and urine (*e.g.*, major components in soil and lake water: Cl^-, SO_4^{2-}, and humic acid; major components in urine: Na^+, K^+, Cl^-, SO_4^{2-}, and urea). Due to the high affinity between Ag NPs on this SERS substrate and different types of PFASs, the slight differences in the peak positions of Raman signals from different types of PFASs are expected to be easily recognized. Nevertheless, under conditions where multiple PFASs of different types with highly similar structures coexist, shifts in the peak positions of Raman signals can also occur due to competition in principle, making detection and identification based on the PFAS type and concentration difficult. To support the immobilization of specific PFASs onto substrates, Ag NPs have been surface-modified with *p*-phenylenediamine nanoparticles (Park *et al.*[111]), thiol molecules (Rothstein *et al.*[112]), graphene (McDonnell *et al.*[113]), and CD (Li *et al.*[114]), which can interact with specific PFASs (Fig. 6B). On this SERS substrate containing Ag NPs, changes in Raman signals before and after the addition of PFOA or PFOS in water (and in methanol, in some cases) could be immediately detected and identified, achieving a LOD of 0.4–40 ppt. The SERS substrate[111] containing Ag NPs surface-modified with *p*-phenylenediamine nanoparticles could instantly distinguish changes in the peak positions of Raman signals before and after addition of PFOA in water, achieving a LOD of 0.53 ppt. The reactivity toward inorganic anions (primary constituents in tap water: Cl^-, SO_4^{2-}, and others) was evaluated, though it had minimal impact on the detection of specific PFASs. The Ag NPs on this SERS substrate readily interact with different types of PFASs, making it easier to recognize the slight differences in the peak positions of Raman signals from different PFASs. On the other hand, under conditions where multiple PFASs of different types with similar structures coexist, shifts in the peak positions of Raman signals are also expected to occur due to competition in principle, making detection and identification based on the sPFAS type and concentration difficult. SERS substrates containing thiol molecules,[112] graphene,[113] and CD[114]-surface-modified Ag NPs could instantly distinguish changes in the peak positions of Raman signals before and after addition of PFOA or PFOS in water (some in methanol), with a LOD ranging from 0.4 to 40 ppt. The effect of contaminants on these SERS substrates had not been evaluated. The Ag NPs on these SERS substrates also interact readily with each type of PFAS, making it easier to recognize the slight differences in the peak positions of Raman signals from different PFASs. Nonetheless, under conditions where multiple structurally similar PFASs coexist, shifts in the peak positions of Raman signals are also expected to occur due to fundamental competition, making detection and identification based on the PFAS type and concentration difficult.

In many cases, the effects of contaminants (*e.g.*, ions, surfactants, and dissolved organic matter) on detection performance remain to be clarified. Besides, there are fewer examples of detection and identification of PFAS species other than PFOA and PFOS compared to other studies. These research, based on slight differences in the peak positions of Raman signals corresponding to different types of PFASs with highly similar structures, indicate that under conditions where multiple PFASs coexist, shifts in the peak positions of Raman signals can also occur due to competition; therefore, while further consideration is necessary, it is highly possible that detection and identification will become difficult depending on the type and concentration of PFASs. To apply this method for on-site detection in actual aqueous environments, it is necessary to verify changes in the peak positions of Raman signals under conditions where various PFASs are present, as well as the feasibility of identifying target PFASs from aqueous environments containing multiple PFASs and contaminants.

3. Conclusion

Although regular monitoring of specific PFASs in aqueous environments is being prioritized worldwide, LC-MS/MS remains the only technique capable of detecting and identifying specific PFASs at the ppt level. However, LC-MS/MS is expensive, time-intensive, and inaccessible to non-experts, rendering it unsuitable for assessing potentially contaminated water sources. This review outlines rapid and sensitive detection research based on nano-level interaction with specific PFASs that can overcome the challenges of LC-MS/MS. Detection methods for specific PFASs can be divided into colorimetric (section 2.1), fluorescence (section 2.2), electrochemical (section 2.3), and SERS (section 2.4)-based methods. The corresponding detection mechanisms and optimization methods to improve detection sensitivity, along with LOD values, are summarized (Table 1: colorimetric, Table 2: fluorescence, Table 3: electrochemical, and Table 4: SERS). These detection research studies enable the detection of specific PFASs in a short time (within several minutes to hours) compared with LC-MS/MS, which requires half a day to more than a day of measurement time. However, among the major specific PFAS detection research studies summarized, few were able to detect several ppt levels in actual aqueous environments. Furthermore, due to challenges such as undesirable reactions and interactions caused by contaminants, as well as the difficulty of detecting and identifying only the target PFASs in aqueous environments with varying pH levels where multiple PFASs and contaminants coexist, consequently, most research based on nano-level interactions with specific PFASs has not advanced to verification research for use in actual on-site detection (selective detection of specific PFASs at several ppt levels in aqueous environments with different pH levels containing contaminants such as ions and dissolved organic matter).

4. Future prospects for detection research based on nano-level interactions

While diverse technologies based on nano-level interactions are being explored for detecting trace specific PFASs, each method faces specific challenges. Colorimetric detection (section 2.1) of specific PFASs was performed primarily in water (without SPE) and was able to detect PFOA, PFOS, and other PFASs at several ppb–ppm levels; however, this method has not achieved detection of PFAS at regulatory levels (several ppt levels) established in countries worldwide. For this reason, it is urgent to achieve the LOD at the ppt level for PFAS-responsive dyes by combining surface modification with substituents that enhance interactions with PFAS (*e.g.*, perfluoroalkyl chains capable of F–F interactions[76] and quaternary ammonium groups enabling electrostatic interactions[115]) and expansion of the PFAS-responsive site (*e.g.*, introduction of cavity structures or increasing specific surface area through porosity). Due to the influence of contaminants such as ions found in tap water or river water and surfactants with structures similar to specific PFASs, some detection materials recommend removing contaminants *via* SPE prior to detection of PFASs. Due to the evaluation of changes in absorbance and absorption spectrum at the same wavelength, it is expected to be difficult to distinguish different types and concentrations of PFASs in the presence of multiple PFASs using this method. Research on colorimetric detection for on-site detection (with SPE) is also underway, and PFOA or PFOS were successfully detected based on the colour tones of the hydrophobic ion pairs formed between the extracted PFOA or PFOS and a dye in ethyl acetate. However, even with prolonged SPE, contaminants cannot be completely removed, making it impossible to detect specific PFASs at the ppt level. Furthermore, it necessitates the use of ethyl acetate that cannot be disposed of as general waste when detecting specific PFASs. By introducing perfluoroalkyl chains[76] of varying carbon chain lengths capable of identifying different types of PFASs into dyes used for colorimetric detection verification research, it is potentially possible to suppress reactivity with inorganic anions and achieve identification of target PFASs in aqueous environments where multiple PFASs coexist. However, many dyes incorporating perfluoroalkyl chains are not water-soluble, making it impossible to directly detect PFASs in water; therefore, detection and identification of PFASs must be performed in organic solvents where the dyes are soluble.

Fluorescence detection (Section 2.2) enables the highly sensitive detection of PFOA, PFOS, and other PFASs at the ppt–ppb levels, primarily in water (without SPE) compared to colorimetric detection. This method showed LODs for PFAS detection that are close to regulatory levels (several ppt levels) set around the world. However, for detection materials with LODs close to the ppt level, the quantitation capabilities of specific PFASs tend to be compromised due to the influence of ions that readily coordinate with the terminal functional groups of

specific PFASs found in tap water or river water, as well as contaminants from surfactants with structures similar to specific PFASs. Therefore, it is necessary to remove contaminants that reduce the quantification abilities of specific PFASs using SPE, and the formation of multi-point interactions through simultaneous modification with substituents (*e.g.*, perfluoroalkyl chains[76] and quaternary ammonium groups enabling electrostatic interactions[115]) that are less susceptible to contaminants and more likely to interact with specific PFASs, incorporation of biological recognition elements (*e.g.*, enzymes, antibodies, or aptamers),[116] and the improvement of dispersion stability for detection materials using surfactants structurally dissimilar to PFASs (*e.g.*, surfactin,[117–120] organometallic nonclassical surfactants,[121] and bolaamphiphile surfactants[122]) are required. Because the 'turn-off type' and 'turn-on type' evaluate changes in fluorescence intensity at the same wavelength, it is expected that these detection materials will also have difficulty distinguishing between different PFAS in the presence of multiple PFASs. Based on the intensity ratio of different fluorescent wavelengths, the 'ratiometric type' is expected to enable detection and identification of PFAS types and concentrations in the coexistence of multiple PFASs. Furthermore, on-site application of this research requires a large number of high-resolution portable fluorometers (USD 20 000–30 000) for detecting specific PFASs, making the widespread use in aqueous environments impractical. Similar to colorimetric detection, verification research of fluorescence detection (with SPE) for on-site detection is also underway, and PFOA or PFOS extracted with in methanol were successfully detected using a composite sensor consisting of a CD derivative and an indicator molecule (dye). However, even with long-term SPE, it is not possible to completely remove contaminants, making it impossible to detect specific PFASs at the ppt level. Furthermore, it cannot identify PFASs other than PFOA (such as fluorotelomers or aqueous film-forming foam). Furthermore, methanol, which cannot be disposed of as general waste, must be used during the implementation of SPE and the detection of specific PFASs. In the verification research of fluorescence detection for on-site detection, since the detection technology relies on changes in fluorescence intensity at the same wavelength, it is anticipated that detecting and identifying the target PFASs from aqueous environments where multiple PFASs coexist will be difficult.

The electrodes used in electrochemical detection (section 2.3) enabled high-sensitivity detection of PFOA, PFOS, and other PFASs at ppt–ppb levels in buffers containing specific PFASs (*e.g.*, PBS and $KHCO_3$) (without SPE). This method showed LODs for PFAS detection that are close to regulatory levels (several ppt levels) set around the world. However, some electrodes with LODs close to the ppt level are susceptible to interference from contaminants such as Na^+ and Cl^-, which are likely to competitively adsorb onto electrode surfaces through interactions similar to those with PFASs; humic acid, a representative dissolved organic compound; as well as SDS and SDBS, which have structures similar to specific PFASs; consequently, the quantification capabilities of specific PFASs is easily reduced. Therefore, it is necessary to remove contaminants that reduce the quantitative accuracy of specific PFASs using SPE, and the surface design combining the formation of multi-point interactions through simultaneous modification with substituents (*e.g.*, perfluoroalkyl chains with carbon chain lengths as short as those of PFASs with short carbon chains[76] and quaternary ammonium groups enabling electrostatic interactions[115]) that are less susceptible to contaminants on the electrode and readily interact with PFASs (especially PFASs with short carbon chains) and the incorporation of PFAS-templated nanostructures (especially PFASs with medium to long carbon chain lengths that readily form nanosized templates) is required. There are issues such as the need for a supporting electrolyte for all electrochemical measurements and limitations on use in areas where power supply is unstable. Among these, research on forming nanosized templates on the electrode surface has been able to control the detection ability of different types of PFASs; therefore, by combining this material with surface modification of substituents that easily interact with PFASs, it is expected that detection and identification will be possible based on the type and concentration of PFASs in the coexistence of multiple PFASs.

The SERS substrates containing Ag NPs used for SERS detection (section 2.4) was able to detect PFOA, PFOS, and other PFASs mainly in water with high sensitivity at the ppt–ppb level based on slight differences in the peak positions of Raman signals. This method showed LODs for PFAS detection that are close to regulatory levels (several ppt levels) set around the world. The few studies evaluating the effect of contaminants on the developed SERS substrate did not show the effect of contaminants such as ions and dissolved organic matter present in tap water, soil water, lake water, and urine. In many cases, the effect of contaminants on SERS substrates remains unvalidated; therefore, SERS substrates exhibiting ppt-level LODs must be closely monitored to ensure that the quantification capabilities of specific PFASs do not decrease in the presence of contaminants. If the SERS substrate is affected by contaminants, it will be necessary to remove the contaminants by SPE, which will reduce the quantification capabilities of specific PFASs, and simultaneous modification of the SERS substrate with multiple substituents (*e.g.*, perfluoroalkyl chains[76] and quaternary ammonium groups enabling electrostatic interactions[115]) that are less susceptible to contaminants and more likely to interact with specific PFASs, and surface modification with compounds that balance the affinity between different PFASs (amphiphilic self-assembled monolayer or polymer brushes containing both cationic and hydrophobic domains[123,124]), or selective host molecules (*e.g.*, β-CD and calixarenes[125,126]) are required. This method relies on slight differences in peak positions of Raman signals originating from structurally similar types of PFASs; consequently, in the presence of multiple PFASs, shifts in the peak positions of Raman signals can also occur due to competition, making detection and identification based on the PFAS type and concentration inherently difficult.

Among the four major detection research covered in this review, all except colorimetric detection have achieved the

detection and quantification of specific PFASs at the ppt level. However, due to detection mechanisms based on nano-level interactions with specific PFASs, detection materials with lower LODs (ppt level) within each research were easily affected by contaminants such as ions, surfactants, and dissolved organic matter, which reduces the quantitative accuracy of specific PFASs. Moreover, in most experiments, aqueous solutions containing dissolved PFOA or PFOS alone have been used. To date, there have been few research on (1) selective detection and quantification of PFOA or PFOS (each as a single substance) from aqueous environments containing contaminants, and (2) selective detection and quantification of the target PFASs from mixed solutions containing various PFASs. In the major detection research, several technologies have been found to be able to detect different types of PFASs (each as a single substance) by utilizing the nano-level interactions between PFASs and the surface of detection materials (colorimetric detection: F–F interactions,[64] fluorescence detection: hydrophobic interactions,[95] electrochemical detection: selective adsorption to templates on the material surface,[106] and SERS detection: differences in Raman signal wavelengths derived from the vibration of C–F bonds in various PFASs[109]). These detection research studies exhibit some responsiveness to contaminants (SERS detection alone is often untested), although their effect is smaller compared to the responsiveness observed during PFAS detection. Therefore, it is highly anticipated that (1) selective detection and quantification of PFOA or PFOS (each as a single substance) from aqueous environments containing contaminants is feasible without SPE. Meanwhile, much of current research capable of detecting multiple types of PFASs (each as a single substance) relies on changes in absorbance or fluorescence intensity at the same wavelength, or slight changes in electrical or Raman signals. Hence, (2) selective detection and quantification of the target PFASs from mixed solutions containing various PFASs is considered difficult to achieve due to competitive or cancelling interactions between different types of PFASs and the detection material. (Different types of PFASs cannot be identified, and the decrease in quantitative accuracy is expected.) To achieve selective detection and quantification of the specific PFASs in (2), it is necessary to develop materials where the wavelengths of absorption, fluorescence, and Raman signals vary significantly depending on the type of PFAS, as well as electrodes where the degree of interaction changes substantially according to the type of PFAS. To use future PFAS detection research in actual aqueous environments, it is necessary to incorporate the latest findings outlined in this review into material design and achieve detection and quantification of PFASs without SPE under conditions (water containing a mixture of multiple PFASs, inorganic anions, and dissolved organic matter, among others) resembling actual aqueous environments, such as those described in (1) and (2).

In perspectives of on-site analysis of actual aqueous environments, given the trend toward stricter regulations on specific PFASs in various countries around the world (increase in the number of PFAS types subject to regulation and further reduction of permissible concentrations in water[127]), it is important (the necessary requirements) to be able to quickly detect, quantify, and identify multiple PFASs in the extensive water bodies using a simple method. However, the major research outlined in this review has the challenge of failing to meet the following requirements for on-site analysis of actual water environments. Colorimetric detection: detecting and quantifying PFAS at regulatory ppt levels; establishing technology that do not use SPE and organic solvents. Fluorescence detection: identification and quantification of target PFASs from water containing multiple PFASs and contaminants; establishment of technology not requiring SPE and organic solvents. Electrochemical detection: selective PFAS detection and quantification in the presence of contaminants; identification and quantification of target PFASs from water containing multiple PFASs; securing stable power sources across wide areas; preparation of optimal supporting electrolytes for each water body. SERS detection: detection and quantitative capabilities for various PFAS species remain unclear; detection and quantitative capabilities for PFASs in the presence of contaminants remain unclear; development of SERS substrates required for the highly sensitive detection, quantification, and identification of different types of PFASs.

To carry out on-site analysis of actual water environments over extensive water bodies, the developed detection technology must be portable so that it can be easily used in each water body. In fact, label-free optical PFAS detection technology is being investigated as an emerging technology for portable specific PFAS detection.[128–130] While these portable technologies have the potential to become platforms for specific PFAS detection due to their low power consumption, they have challenges such as insufficient LODs (hundreds of ppt to a few ppb), unknown effects on contaminants, and the need for high levels of expertise in each portable technology (device setup). Although each detection research is beginning to obtain promising results indicating its potential to detect, quantify, and identify multiple PFASs, setting up new equipment tailored to each detection research for portability – a requirement for conducting on-site analysis across extensive water bodies – could become a barrier to adoption. Conversely, inexpensive portable spectrophotometers for water quality analysis, necessary for implementation in extensive water bodies, are actually being used at each site.[131–134] Therefore, among the verification research studies outlined in this review, if the technology capable of detecting and quantifying ppt-level PFASs in colorimetric detection without using SPE and organic solvents can be established and the requirements for on-site analysis of actual water environments can be met, it is expected that combining this technology with portable spectrophotometers will bring us the closest to quickly realizing on-site detection in aqueous environments across the country, where regulations on specific PFASs are being strengthened.

Author contributions

Aki Shibata: data curation, funding acquisition, investigation and writing – original draft & editing. Mitsuaki Nuno: data

curation, funding acquisition, investigation and writing – review & editing. Tomoka Ishikawa: data curation and investigation. Hitoshi Kasai: data curation, funding acquisition and writing – review & editing. Kouki Oka: conceptualization, data curation, funding acquisition, investigation, supervision, and writing – original draft and review & editing.

Conflicts of interest

The author declares no competing financial interest.

Data availability

No primary research results, software or code have been included and no new data were generated or analyzed as part of this feature article.

Acknowledgements

This work was supported by the New Energy and Industrial Technology Development Organization (NEDO), Japan, under the Leading Research Program (No. JPNP14004) and the JSPS Grants-in-Aid for Scientific Research (No. JP23H03827, JPJSBP120258801, JP24K01552, JP25K21722, JP22H00328, JP24KF0174, JP25K00058 and JP25K23579) from MEXT, Japan. In addition, this work was partially supported by the Environment Research and Technology Development Fund (JPMEERF20241RA4, 5RB-2502) of the Environmental Restoration and Conservation Agency provided by the Ministry of the Environment of Japan. Kouki Oka also acknowledges the support from the Amano Industry Technology Laboratory, the Ozawa and Yoshikawa Memorial Electronics Research Foundation, the Noguchi Institute (NJ202411), the TEPCO Memorial Foundation, the Fujimori Science and Technology Foundation, the Paloma Environmental Technology Development Foundation, the Intelligent Cosmos Academic Foundation, the Kato Foundation for Promotion of Science (KS-3416), Sugiyama Houkoukai, the Shorai Foundation for Science and Technology, the Yamada Science Foundation, the Kenjiro Takayanagi Foundation, the Kansai Research Foundation for Technology Promotion, the Yashima Environment Technology Foundation, the JACI Prize for Encouraging Young Researchers, the Iketani Science and Technology Foundation, and the Foundation for Interaction in Science & Technology. Aki Shibata also acknowledges the support from the Yamaguchi Educational and Scholarship Foundation and the Mishima Kaiun Memorial Foundation.

References

1 Z. Wang, A. M. Buser, I. T. Cousins, S. Demattio, W. Drost, O. Johansson, K. Ohno, G. Patlewicz, A. M. Richard, G. W. Walker, G. S. White and E. Leinala, *Environ. Sci. Technol.*, 2021, **55**, 15575–15578.
2 I. T. Cousins, J. C. DeWitt, J. Gluge, G. Goldenman, D. Herzke, R. Lohmann, M. Miller, C. A. Ng, M. Scheringer, L. Vierke and Z. Wang, *Environ. Sci.: Processes Impacts*, 2020, **22**, 1444–1460.
3 X. Jiang, Y. Luo, S. Mu, B. Meng, W. Wang, G. Yu and S. Deng, *Water Res.*, 2025, **268**, 122749.
4 D. M. Wanninayake, *J. Environ. Manage.*, 2021, **283**, 111977.
5 Z.-W. Ke, S.-J. Wei, P. Shen, Y.-M. Chen and Y.-C. Li, *Appl. Clay Sci.*, 2023, **232**, 106804.
6 J. Li, B. Xi, G. Zhu, Y. Yuan, W. Liu, Y. Gong and W. Tan, *Environ. Res.*, 2023, **218**, 114980.
7 R. Akai, H. Kasai and K. Oka, *Nanoscale*, 2025, **17**, 9920–9925.
8 T. Ami, K. Oka, S. Kitajima and N. Tohnai, *Angew. Chem., Int. Ed.*, 2024, **63**, e202407484.
9 T. Ami, K. Oka, K. Tsuchiya and N. Tohnai, *Angew. Chem., Int. Ed.*, 2022, **61**, e202202597.
10 X. Liu, S. Liu, W. Qiu, J. T. Magnuson, Z. Liu, G. Yang, H. Chen, Y. Li, X. Xu and C. Zheng, *Sustain. Horiz.*, 2022, **3**, 100027.
11 A. A. Bayode, S. S. Emmanuel, A. O. Akinyemi, O. T. Ore, S. O. Akpotu, D. T. Koko, D. E. Momodu and E. A. Lopez-Maldonado, *Environ. Res.*, 2024, **261**, 119719.
12 Y. Wang, S. B. Darling and J. Chen, *ACS Appl. Mater. Interfaces*, 2021, **13**, 60789–60814.
13 M. Yadav, F. J. Osonga and O. A. Sadik, *Sci. Total Environ.*, 2024, **912**, 169279.
14 K. A. Barzen-Hanson, S. C. Roberts, S. Choyke, K. Oetjen, A. McAlees, N. Riddell, R. McCrindle, P. L. Ferguson, C. P. Higgins and J. A. Field, *Environ. Sci. Technol.*, 2017, **51**, 2047–2057.
15 A. B. Lindstrom, M. J. Strynar and E. L. Libelo, *Environ. Sci. Technol.*, 2011, **45**, 7954–7961.
16 D. Herzke, E. Olsson and S. Posner, *Chemosphere*, 2012, **88**, 980–987.
17 Q. Li, T. Wang, Z. Zhu, J. Meng, P. Wang, S. Suriyanarayanan, Y. Zhang, Y. Zhou, S. Song, Y. Lu and B. Yvette, *Chemosphere*, 2017, **167**, 344–352.
18 S. K. Nayak, K. Bhardwaj, P. K. Verma and S. Yamijala, *J. Phys. Chem. Lett.*, 2025, **16**, 8046–8055.
19 S. Kurwadkar, J. Dane, S. R. Kanel, M. N. Nadagouda, R. W. Cawdrey, B. Ambade, G. C. Struckhoff and R. Wilkin, *Sci. Total Environ.*, 2022, **809**, 151003.
20 X. Lei, Q. Lian, X. Zhang, T. K. Karsili, W. Holmes, Y. Chen, M. E. Zappi and D. D. Gang, *Environ. Pollut.*, 2023, **321**, 121138.
21 W. Tang, Y. Meng, B. Yang, D. He, Y. Li, B. Li, Z. Shi and C. Zhao, *J. Environ. Sci.*, 2022, **122**, 14–24.
22 J. Sun, X. Jiang, H. Xiang, X. Wang, X. Luo, J. Fu and J. Fan, *J. Environ. Chem. Eng.*, 2024, **12**, 113210.
23 D. Lu, S. Sha, J. Luo, Z. Huang and X. Z. Jackie, *J. Hazard. Mater.*, 2020, **386**, 121963.
24 Q. Wang, Y. Shao, K. M. Y. Leung, P. K. S. Lam and Y. Ruan, *Mar. Pollut. Bull.*, 2025, **216**, 117993.

25 Y. Cui, S. Wang, D. Han and H. Yan, *TrAC, Trends Anal. Chem.*, 2024, **176**, 117754.
26 P. Wang, G. An, I. Carra, F. Hassard, P. C. Moreno, H. Sakar, M. Jodkowska, D. Wang, B. Jefferson, W. Chu and P. Jarvis, *Sep. Purif. Technol.*, 2025, **355**, 129562.
27 S. Y. Wee and A. Z. Aris, *npj Clean Water*, 2023, **6**, 57.
28 R. F. Menger, E. Funk, C. S. Henry and T. Borch, *Chem. Eng. J.*, 2021, **417**, 129133.
29 C. S. Skaggs and B. A. Logue, *J. Chromatogr. A*, 2021, **1659**, 462493.
30 G. W. Olsen, D. C. Mair, C. C. Lange, L. M. Harrington, T. R. Church, C. L. Goldberg, R. M. Herron, H. Hanna, J. B. Nobiletti, J. A. Rios, W. K. Reagen and C. A. Ley, *Environ. Res.*, 2017, **157**, 87–95.
31 M. D. Firouzjaei, E. Zolghadr, S. Ahmadalipour, N. Taghvaei, F. A. Afkhami, S. Nejati and M. A. Elliott, *Environ. Chem. Lett.*, 2021, **20**, 661–679.
32 A. Adewuyi and Q. Li, *Eco-Environ. & Health*, 2024, **3**, 355–368.
33 J. L. Domingo and M. Nadal, *Environ. Res.*, 2019, **177**, 108648.
34 S. Y. Wee and A. Z. Aris, *Ecotoxicol. Environ. Saf.*, 2023, **267**, 115663.
35 Y. Deng, Z. Liang, X. Lu, D. Chen, Z. Li and F. Wang, *Chemosphere*, 2021, **283**, 131168.
36 K. Steenland, T. Fletcher, C. R. Stein, S. M. Bartell, L. Darrow, M. J. Lopez-Espinosa, P. B. Ryan and D. A. Savitz, *Environ. Int.*, 2020, **145**, 106125.
37 V. Barry, A. Winquist and K. Steenland, *Environ. Health Perspect.*, 2013, **121**, 1313–1318.
38 A. R. Tursi, B. Lindeman, A. B. Kristoffersen, H. Hjertholm, E. Bronder, M. Andreassen, T. Husoy, H. Dirven, S. Andorf and U. C. Nygaard, *Environ. Res.*, 2024, **256**, 119221.
39 J. C. DeWitt, M. M. Peden-Adams, J. M. Keller and D. R. Germolec, *Toxicol. Pathol.*, 2012, **40**, 300–311.
40 X. Du, Y. Wu, G. Tao, J. Xu, Z. Du, M. Wu, T. Gu, J. Xiong, S. Xiao, X. Wei, Y. Ruan, P. Xiao, L. Zhang and W. Zheng, *Sci. Total Environ.*, 2024, **953**, 175958.
41 C. Lau, J. R. Thibodeaux, R. G. Hanson, M. G. Narotsky, J. M. Rogers, A. B. Lindstrom and M. J. Strynar, *Toxicol. Sci.*, 2006, **90**, 510–518.
42 A. E. Lindell, A. Griesshammer, L. Michaelis, D. Papagiannidis, H. Ochner, S. Kamrad, R. Guan, S. Blasche, L. N. Ventimiglia, B. Ramachandran, H. Ozgur, A. Zelezniak, N. Beristain-Covarrubias, J. C. Yam-Puc, I. Roux, L. P. Barron, A. K. Richardson, M. G. Martin, V. Benes, N. Morone, J. E. D. Thaventhiran, T. A. M. Bharat, M. M. Savitski, L. Maier and K. R. Patil, *Nat. Microbiol.*, 2025, **10**, 1630–1647.
43 V. Polychronidou and R. Nag, *Sci. Total Environ.*, 2025, **1000**, 180428.
44 H. Fiedler, *Environ. Health*, 2023, **1**, 41–52.
45 Q. Wenhui, Y. Ge, C. Ling, N. Shan, L. Yuzhe, F. Di, D. Zhaomin, T. M. Jason, S. Daniel, M. Y. L. Kenneth, Z. Yi, Z. Zhenzhong, F. Lian, Z. Xianming, Z. Yanxu, F. Wenhong, H. Tao, M. Jianmin, W. Minghong, T. Shu and Z. Chunmiao, *Science*, 2025, **390**, 1305–1309.
46 M. G. Evich, M. J. B. Davis, J. P. McCord, B. Acrey, J. A. Awkerman, D. R. U. Knappe, A. B. Lindstrom, T. F. Speth, C. Tebes-Stevens, M. J. Strynar, Z. Wang, E. J. Weber, W. M. Henderson and J. W. Washington, *Science*, 2022, **375**, eabg9065.
47 H. Mezawa, A. Eguchi, M. Yamamoto, N. Tokuda, M. Shima, S. Nakayama, M. Kamijima and Japan Environment and Children's Study Group, *Environ. Int.*, 2025, **204**, 109824.
48 A. Y. Lin, S. C. Panchangam and C. C. Lo, *Environ. Pollut.*, 2009, **157**, 1365–1372.
49 G. R. Johnson, M. L. Brusseau, K. C. Carroll, G. R. Tick and C. M. Duncan, *Sci. Total Environ.*, 2022, **841**, 156602.
50 Q. A. Al-Maqtari, A. A. Mahdi, N. Othman, A. E. Noman, L. M. Alsubhi, W. AlAnsi, S. M. Asharuddin, M. K. Talib, S. Supramanium and A. Al-Gheethi, *Results Eng.*, 2025, **28**, 107169.
51 Z. Dong, G. Ji, F. Wang and F. Wang, *J. Environ. Chem. Eng.*, 2025, **13**, 118145.
52 E. Southerland and L. S. Birnbaum, *Environ. Sci. Technol.*, 2023, **57**, 7103–7105.
53 X. Li, M. Fatowe, D. Cui and N. Quinete, *Sci. Total Environ.*, 2022, **806**, 150393.
54 M. Mann, V. Kartseva, C. Stanley, M. Blumenthal, R. Silliboy and B. Berger, *RSC Sustainability*, 2024, **2**, 3967–3972.
55 C. Gao, D. S. Drage, M. A.-E. Abdallah, F. Quan, K. Zhang, S. Hu, X. Zhao, Y. Zheng, S. Harrad and W. Qiu, *ACS ES&T Water*, 2024, **4**, 4881–4892.
56 X. Jin, Z. Wang, R. Hong, Z. Chen, B. Wu, S. Ding, W. Zhu, Y. Lin and C. Gu, *Water Res.*, 2022, **225**, 119147.
57 E. Gagliano, M. Sgroi, P. P. Falciglia, F. G. A. Vagliasindi and P. Roccaro, *Water Res.*, 2020, **171**, 115381.
58 D. Thompson, N. Zolfigol, Z. Xia and Y. Lei, *Sens. Actuators Rep.*, 2024, **7**, 100189.
59 M. Renaud-Young, J. Guegueniat, S. Chaudhuri, M. S. Stietz, E. C. Hicks and R. M. Mayall, *Ground Water Monit. Rev.*, 2025, **45**, 34–36.
60 A. U. Rehman, M. Crimi and S. Andreescu, *Trends Environ. Anal. Chem.*, 2023, **37**, e00198.
61 B. Qian, J. L. Rayner, G. B. Davis, A. Trinchi, G. Collis, I. L. Kyratzis and A. Kumar, *Ecotoxicol. Environ. Saf.*, 2024, **284**, 116932.
62 Z. Zheng, H. Yu, W. C. Geng, X. Y. Hu, Y. Y. Wang, Z. Li, Y. Wang and D. S. Guo, *Nat. Commun.*, 2019, **10**, 5762.
63 J. Ma, C. Liu, J. Li, Z. An, B. Zhang, W. Hong, C. Ye, M. Li and L.-H. Guo, *Environ. Sci. Nano*, 2025, **12**, 1581–1591.
64 J. Jung, J. Park, J. K. Choe and Y. Choi, *Water Res.:X*, 2024, **24**, 100239.
65 X. Xu, M. Ma, X. Zhou, X. Zhao, D. Feng and L. Zhang, *ACS Appl. Mater. Interfaces*, 2024, **16**, 15959–15969.
66 Y. Yang, H. Sun, T. Han, Q. Hao, H. Shen, Y. Jing, X. Liu, S. Mu and H. Zhang, *Anal. Chem.*, 2025, **97**, 10474–10483.

67 N. Yang, X. Lin, X. Zheng, W. Lai, Y. Lin, Z. Zou, Q. Wang and X. Zheng, *Mikrochim. Acta*, 2025, **192**, 134.
68 Q. Liu, Q. Chen, Y. J. Tong, X. Zou, X. Zheng and Z. Gong, *Anal. Chem.*, 2024, **96**, 4673–4681.
69 C. Hou, F. Chen, D. Cheng, S. Zou, J. Wang, M. Shen and Y. Wang, *Chem. Eng. J.*, 2024, **481**, 148467.
70 Q. An, Y. Tan, X. Du, H. Fu, P. J. J. Alvarez and X. Qu, *Sens. Actuators, B*, 2026, **448**, 138926.
71 Y. Cui, N. Zhao, Y. Chen, S. Wang, H. Yan and D. Han, *Mikrochim. Acta*, 2025, **192**, 356.
72 H. Zhao, W. Xue, L. Wang, L. Zhang and X. Xu, *ChemNanoMat*, 2025, **11**, e202500164.
73 T. Y. Guo, H. W. Li, C. X. Zhang and Y. Wu, *Analyst*, 2023, **148**, 3931–3937.
74 Y. Wang, Y. Chen, Q. Meng, R. Ren, L. Jing, H. Li, L. Zhou, Z. Tian, J. Wang and C. Hou, *Sep. Purif. Technol.*, 2024, **332**, 125824.
75 J. Liu, X. Wang, F. Ma, X. Yang, Y. Liu, X. Zhang, S. Guo, Z. Wang, S. Yang and R. Zhao, *Chem. Eng. J.*, 2022, **435**, 134966.
76 C. M. Taylor, M. C. Breadmore and N. L. Kilah, *Sens. Diagn.*, 2023, **2**, 676–686.
77 C. M. Taylor, T. A. Ellingsen, M. C. Breadmore and N. L. Kilah, *Chem. Commun.*, 2021, **57**, 11649–11652.
78 C. M. Taylor, M. C. Breadmore, N. L. Kilah and C. Wentrup, *Aust. J. Chem.*, 2023, **76**, 709–718.
79 R. F. Menger, J. J. Beck, T. Borch and C. S. Henry, *ACS ES&T Water*, 2022, **2**, 565–572.
80 C. Fang, X. Zhang, Z. Dong, L. Wang, M. Megharaj and R. Naidu, *Chemosphere*, 2018, **191**, 381–388.
81 M. Al Amin, Z. Sobhani, S. Chadalavada, R. Naidu and C. Fang, *Environ. Technol. Innovation*, 2020, **18**, 100778.
82 L. Jiang, Z. Huang, J. Xu, L. Zhang and Z. Du, *Chem. Eng. J.*, 2024, **484**, 149355.
83 L. Chun-Ze, A. F. Melissa, C. C. Rosenildo, A. G. John, S. Andreas and B. Philippe, *Anal. Chem.*, 2010, **82**, 7634–7640.
84 R. Dalapati, S. Manickam, J. Shi, M. Hunter and L. Zang, *Anal. Chim. Acta*, 2025, **1341**, 343670.
85 C. Zhao, S. Hussain, J. Li, C. Liu, M. A. Afroz, C. Zhu, Z. Yue, J. Zhang, Y. Hao and R. Gao, *Anal. Chem.*, 2025, **97**, 10027–10037.
86 R. Dalapati, M. Hunter, M. Sk, X. Yang and L. Zang, *ACS Appl. Mater. Interfaces*, 2024, **16**, 32344–32356.
87 R. Dalapati, J. Shi, M. Hunter and L. Zang, *J. Mater. Chem. C*, 2025, **13**, 16753–16762.
88 M. H. Hassan, R. Khan, D. Andreescu, S. Shrestha, M. Cotlet and S. Andreescu, *Adv. Funct. Mater.*, 2024, **34**, 2403364.
89 E. Xu, C. Long, Y. Qiao, Z. Chen, X. Yang and P. Ren, *Inorg. Chem.*, 2025, **64**, 19697–19704.
90 S. Mohammadi, C. Sandoval-Pauker, Z. N. Dorado, T. P. Senftle, R. Pankow and H. Sharifan, *Anal. Chem.*, 2025, **97**, 10075–10084.
91 S. Mohammadi, Z. N. Dorado and H. Sharifan, *ACS Appl. Nano Mater.*, 2024, **7**, 21410–21419.
92 A. Concellón, J. Castro-Esteban and T. M. Swager, *J. Am. Chem. Soc.*, 2023, **145**, 11420–11430.
93 Y. Yang, X. Liu, B. Mu, S. Meng, S. Mao, W. Tao and Z. Li, *Biosens. Bioelectron.*, 2024, **257**, 116330.
94 J. Wang, X. Wan, W. Li, C. Song, Q. Gao, Q. Pan and Y. He, *Mikrochim. Acta*, 2025, **192**, 563.
95 X. Chen, S. Hussain, Y. Tang, X. Chen, S. Zhang, Y. Wang, P. Zhang, R. Gao, S. Wang and Y. Hao, *Sci. Total Environ.*, 2023, **860**, 160467.
96 R. Mayall, M. Stietz, M. Renaud-Young, J. Guegueniat, A. Woods and C. Chen, *CA Patent*, WO2025/123135A1, 2025.
97 R. M. Mayall, M. Renaud-Young, C. Chen, M. Mcdonald, S. S. Garcia and E. C. Hicks, *CA Patent*, WO2024/216380A1, 2024.
98 M. M. Shanbhag, N. P. Shetti, A. Daouli, M. N. Nadagouda, M. Badawi and T. M. Aminabhavi, *Langmuir*, 2024, **40**, 3831–3847.
99 F. Simonetti, R. Buccini, V. Migliorati, M. Mancini, D. Caterino, V. Gioia, M. Agostini, F. Mazzei, A. Ciccola, G. Favero and R. Zumpano, *Environ. Res.*, 2025, **285**, 122208.
100 J. J. C. Solís, S. Yin, M. Galicia, M. S. Ersan, P. Westerhoff and D. Villagrán, *Chem. Eng. J.*, 2024, **491**, 151821.
101 I. R. Comnea-Stancu and J. F. Staden, *J. Environ. Chem. Eng.*, 2024, **12**, 113850.
102 R. Khan, Z. O. Uygun, D. Andreescu and S. Andreescu, *ACS Sens.*, 2024, **9**, 3403–3412.
103 X. Zheng, C. Li, N. Yang, L. Niu, F. Gao and Q. Wang, *Anal. Chem.*, 2025, **97**, 6347–6358.
104 Y. Xu, Q. Yin, N. Du, Y. Yi and G. Zhu, *Mikrochim. Acta*, 2024, **191**, 693.
105 Y. Gao, W. Gou, W. Zeng, W. Chen, J. Jiang and J. Lu, *Microchem. J.*, 2023, **187**, 108378.
106 N. Amin, J. Chen, Q. He, J. S. Schwartz and J. J. Wu, *Sens. Actuators, B*, 2024, **420**, 136464.
107 M. Pierpaoli, M. Szopinska, A. Olejnik, J. Ryl, S. Fudala-Ksiazek, A. Luczkiewicz and R. Bogdanowicz, *J. Hazard. Mater.*, 2023, **458**, 131873.
108 D. Lu, D. Z. Zhu, H. Gan, Z. Yao, J. Luo, S. Yu and P. Kurup, *Sens. Actuators, B*, 2022, **352**, 131055.
109 Y. Feng, J. Dai, C. Wang, H. Zhou, J. Li, G. Ni, M. Zhang and Y. Huang, *ACS Appl. Nano Mater.*, 2023, **6**, 13974–13983.
110 J. Kumar, A. Jinachandran, V. K. Ponnusamy, G. G. Huang, A. K. Suresh, H. Noothalapati and R. Panneerselvam, *Appl. Surf. Sci.*, 2024, **674**, 160961.
111 H. Park, J. Park, W. Kim, W. Kim and J. Park, *J. Hazard. Mater.*, 2023, **453**, 131384.
112 J. C. Rothstein, J. Cui, Y. Yang, X. Chen and Y. Zhao, *Sens. Diagn.*, 2024, **3**, 1272–1284.
113 C. McDonnell, F. M. Albarghouthi, R. Selhorst, N. Kelley-Loughnane, A. D. Franklin and R. Rao, *ACS Omega*, 2023, **8**, 1597–1605.
114 C. Li, X. Fang, H. Li and X. Zhang, *ACS Appl. Opt. Mater.*, 2024, **2**, 610–616.

115 P. Ramos, S. S. Kalra, N. W. Johnson, C. M. Khor, A. Borthakur, B. Cranmer, G. Dooley, S. K. Mohanty, D. Jassby, J. Blotevogel and S. Mahendra, *Environ. Pollut.*, 2022, **294**, 118603.
116 C. Esposito, A. M. Cusano, T. M. Caputo, A. Aliberti and A. Cusano, *ACS Mater. Lett.*, 2026, **8**, 716–741.
117 T. Taira, S. Yanagisawa, T. Nagano, T. Tsuji, A. Endo and T. Imura, *Colloids Surf., B*, 2017, **156**, 382–387.
118 S. Yanagisawa, T. Imura and T. Taira, *ACS Sustainable Chem. Eng.*, 2023, **11**, 5115–5121.
119 T. Taira, R. Moriyama, K. Sakai, H. Sakai and T. Imura, *Colloids Surf., A*, 2024, **702**, 134989.
120 W. Q. Qin, Y. F. Liu, H. Z. Gang, J. F. Liu, L. Zhou, S. Z. Yang and B. Z. Mu, *Adv. Colloid Interface Sci.*, 2025, **343**, 103581.
121 S. Bitter, M. Kunkel, L. Burkart, A. Mang, R. F. Winter and S. Polarz, *ACS Omega*, 2018, **3**, 8854–8864.
122 S. Stéphanie, R. Kamil, P. Nelly, M. Jean-Daniel, L. V. Nancy, G. Fabienne and M. Christophe, *Chem. Mater.*, 2008, **20**, 1221–1223.
123 N. Faucheux, R. Schweiss, K. Lutzow, C. Werner and T. Groth, *Biomaterials*, 2004, **25**, 2721–2730.
124 F. Frederix, K. Bonroy, W. Laureyn, G. Reekmans, A. Campitelli, W. Dehaen and G. Maes, *Langmuir*, 2003, **19**, 4351–4357.
125 N. M. Y. Zhang, M. Qi, Z. Wang, Z. Wang, M. Chen, K. Li, P. Shum and L. Wei, *Sens. Actuators, B*, 2019, **286**, 429–436.
126 T. S. Vo, T. T. B. C. Vo and K. Kim, *Micro Nano Syst. Lett.*, 2026, **14**, 1–28.
127 K. K. Arun, H. S. Al Yasi, O. Z. Wada, F. AlMomani and K. A. Mahmoud, *Environ. Sci.: Water Res. Technol.*, 2026, **12**, 121–145.
128 N. Cennamo, L. Zeni, P. Tortora, M. E. Regonesi, A. Giusti, M. Staiano, S. D'Auria and A. Varriale, *Talanta*, 2018, **178**, 955–961.
129 F. Faiz, G. Baxter, S. Collins, F. Sidiroglou and M. Cran, *Sens. Actuators, B*, 2020, **312**, 128006.
130 A. V. Saetchnikov, E. A. Tcherniavskaia, V. A. Saetchnikov and A. Ostendorf, *Photonics Res.*, 2023, **11**, A88–A96.
131 S. Sumriddetchkajorn, K. Chaitavon and Y. Intaravanne, *Sens. Actuators, B*, 2014, **191**, 561–566.
132 B. T. Wittbrodt, D. A. Squires, J. Walbeck, E. Campbell, W. H. Campbell and J. M. Pearce, *PLoS One*, 2015, **10**, e0134989.
133 X. Zhu, L. Chen, J. Pumpanen, M. Keinanen, H. Laudon, A. Ojala, M. Palviainen, M. Kiirikki, K. Neitola and F. Berninger, *Talanta*, 2021, **224**, 121919.
134 E. J. Könnel, S. D. Nonno and R. Ulber, *Microchem. J.*, 2025, **214**, 113946.